Bachelor Thesis

ANALYSIS OF THE PERFORMANCE OF A FLEXIBLE WINGLET IN THE PRESENCE OF GUSTS

Author:
Joaquín Gallego Moreno

Director:
Óscar Flores Arias

July 2016

"I've missed more than 9000 shots in my career. I've lost almost 300 games. 26 times, I've been trusted to take the game winning shot and missed. I've failed over and over and over again in my life. And that is why I succeed."

Michael Jordan

Acknowledgments

In first place I want to thank my family for the continuous support and trust. Thanks to my mother, for being an example in every situation of this life, for showing me that it is possible to be happy when you do what you really love. To my Father, for being the best example of an Aerospace Engineer that I could have had. And to my sister, for being able to see always the good side of things and for her continuous love even when I am growling.

I want to thank my friends for having been there since I was a child and in every moment I needed through these four years. Thanks for understanding me in every situation I had to live in this degree. I think it is not necessary to mention them all one by one; they know who they are.

Thanks to all my older degree mates, who apart from being my mates are my friends. I want to thank them all because they helped me in everything they could for completing this thesis.

It may be strange, but I want to thank basketball because it helped me so much for being an Aerospace Engineer. Through this sport, I learned that I have to fight until the end, working with all my capacities, for everything I want; that even when I fight for something until the end, it can go wrong, but I cannot stop, I have to continue. Thanks to this sport, I am the person that I am nowadays.

In special, thanks to Professor Pablo Fajardo for his disinterested and unconditional help through this project, without which I could not have completed this project. Thanks to Oscar for giving me the chance to work with aerodynamics.

Finally, I want to thank Irene for supporting me during these 5 months with her true love, and for showing me how great and funny a person can be.

Abstract

Current aviation faces the paramount challenge of continuing with the actual trend of decreasing the fuel consumption of new generation aircraft. In order to confront such a hurdle, new modern and renewed aircraft designs appear every year. One of these advancements has been the incorporation of the so-called winglets at the aircraft wingtips, which decrease the fuel consumption due to their reduction of the induced Drag.

The objective of the current project is to find the load alleviation that a flexible winglet yields in the presence of gusts. This abatement of the loads can imply a lighter structure, and a consequent decrease of the fuel consumption. The presented model consists on a simplified structural model in which the only variable is the stiffness of a torsion spring which is allocated between the wing and the winglet. In order to accomplish such a goal, the CFD solver CFX is used to compute the aerodynamics.

The final conclusion of the project is that the more flexible the winglet is, the higher assuagement of loads in the presence of a gust is discovered. Besides, it is needed a feasibility study of the implementation of the new proposed design in structural and aeroelastic terms.

Contents

Table of Contents **vii**

List of Figures **ix**

List of Tables **xi**

1 Introduction **1**
- 1.1 Motivation . . . 1
- 1.2 Socio-economic frame . . . 2
- 1.3 Legal framework . . . 3
- 1.4 Gusts . . . 4
  - 1.4.1 Gust calculation . . . 4
  - 1.4.2 Main assumptions . . . 6
- 1.5 The proposed solution . . . 7
- 1.6 Computational tool . . . 8
- 1.7 Project objectives . . . 8
- 1.8 Document overview . . . 9

2 State of the art **11**
- 2.1 Winglets and movable wingtips . . . 11
- 2.2 Morphing wings . . . 13

3 ANSYS CFX solver **15**
- 3.1 Advantages of CFX for the aeronautic industry . . . 15
- 3.2 Turbulence modeling . . . 16

4 Geometry and Mesh **19**
- 4.1 Grid independence study . . . 19
  - 4.1.1 CFX settings . . . 19
  - 4.1.2 Simulations information . . . 21
  - 4.1.3 Grid independence study results . . . 22
  - 4.1.4 Validation of the mesh . . . 22
- 4.2 Geometry . . . 24
  - 4.2.1 Geometry definition . . . 24
  - 4.2.2 Geometric parameters . . . 25
- 4.3 Mesh . . . 26
  - 4.3.1 Mesh domain . . . 26
  - 4.3.2 Mesh characteristics . . . 27
  - 4.3.3 Mesh statistics . . . 30

5 Mathematical procedure 33
5.1 Angles of Attack computation . . . 33
5.1.1 Cruise . . . 33
5.1.2 Gust . . . 33
5.2 Simulations for cruise in CFX . . . 34
5.3 Cant Angle for cruise . . . 34
5.3.1 Moment at the hinge . . . 35
5.4 Simulations for gust in CFX . . . 35
5.5 Passive design mathematical model . . . 35
5.5.1 Model proposition . . . 35
5.5.2 θ_0 calculation . . . 36
5.5.3 Equilibrium Cant Angle . . . 36
5.5.4 Load Factor (n) . . . 37
5.5.5 Evolution with Angle of Attack and time . . . 38
5.6 Active design mathematical model . . . 39

6 Results 41
6.1 Cruise Angle of Attack . . . 41
6.2 Gust Angle of Attack . . . 42
6.3 CFX results . . . 44
6.3.1 Contours of pressure for cruise condition . . . 44
6.3.2 Cruise results . . . 44
6.3.3 Gust results . . . 49
6.4 Passive design analysis . . . 53
6.4.1 Possible drawbacks . . . 59
6.5 Active design analysis . . . 59

7 Project Budget and Planning 63
7.1 Budget . . . 63
7.2 Planning . . . 64

8 Conclusion 67
8.1 Future work . . . 68

Appendices 69

A Additional Figures 71

List of Figures

1.1 Winglet of an A330 aircraft. 1
1.2 Evolution of the fuel consumption in history. 3
1.3 Typical (1-Cosine) Design Gust Velocity Profiles 5
1.4 Wagner function representation 7

2.1 Types of wingtip devices 11
2.2 Passive wingtip dessign 12
2.3 Timeline of aircraft using morphing technology 14

4.1 Sketch of the mesh domains 20
4.2 Final mesh for the grid independence study 21
4.3 Detail of the mesh close to the airfoil 21
4.4 Values of y^+ along the airfoil 23
4.5 Schematic of the wing planform without winglet 24
4.6 Schematic of the winglet planform 24
4.7 Schematic of the winglet angle with respect to the mean line of the wing . . 25
4.8 Final Wing and winglet in ANSYS workbench for a winglet angle of 50 ^{o} . 25
4.9 Mesh domains 26
4.10 Final Mesh 28
4.11 Final mesh focused on the symmetry plane 28
4.12 Region of refinement of the final mesh 29
4.13 Final mesh close to the airfoil 29
4.14 Detail of the mesh on the wing surface 30
4.15 Detail of the inflation layer sorrounding the airfoil 30
4.16 Mesh metrics of the Aspect Ratio 31
4.17 Mesh metrics of the Skewness 32
4.18 Classification of the mesh quality metrics based on skewness 32

5.1 Schematic of the Lift force in the winglet and the point of application . . . 35
5.2 Flowchart for the mathematical computation of the passive case. 38

6.1 Lift coefficient vs Angle of Attack for the VLM results 41
6.2 Evolution of the reference velocities with altitude 42
6.3 Contours of pressure for Cant Angle of 0, 5, 10 ad 20 degrees for Cruise condition. 44
6.4 Variation of the Lift in the wing as a function of the Cant Angle 45
6.5 Variation of the Drag in the wing as a function of the Cant Angle 45
6.6 Variation of the Lift in the winglet as a function of the Cant Angle 46
6.7 Variation of the Drag in the winglet as a function of the Cant Angle 46
6.8 Total Lift as a function of the Cant Angle 47

6.9 Total Drag as a function of the Cant Angle 47
6.10 Aerodynamic efficiency as a function of the Cant Angle 48
6.11 Moment at the hinge as a function of the Cant Angle 48
6.12 Variation of the Lift in the wing for a gust with AoA 11.5° as a function of the Cant Angle 49
6.13 Variation of the Drag in the wing for a gust with AoA 11.5° as a function of the Cant Angle 50
6.14 Variation of the Lift in the winglet for a gust with AoA 11.5° as a function of the Cant Angle 50
6.15 Variation of the Drag in the winglet as a function of the Cant Angle 51
6.16 Total Lift for a gust with AoA 11.5° as a function of the Cant Angle 51
6.17 Total Drag for a gust with AoA 11.5° as a function of the Cant Angle . . . 52
6.18 Moment for a gust with AoA 11.5° as a function of the Cant Angle 52
6.19 Load factor for a gust with AoA 11.5° as a function of the Cant Angle . . . 53
6.20 Natural position(θ_0) of the winglet as a function of the spring rigidity for a cruise Cant Angle of 8.6° 54
6.21 Equilibrium of moments for cruise and gust for the minimum value of K . . 54
6.22 Final Load factor for a gust with AoA 11.5° as a function of the spring rigidity 55
6.23 Final position of the winglet for a gust with AoA 11.5° as a function of the spring rigidity 55
6.24 Load factor alleviation for a gust with AoA 11.5° as a function of the spring rigidity 56
6.25 Load factor change alleviation for a gust with AoA 11.5° as a function of the spring rigidity 56
6.26 Load factor factor evolution with time for a gust of 11.5 ° 57
6.27 Lift coefficient as a function of AoA for rigid and flexible winglet 58
6.28 Load Factor as a function of AoA for rigid and flexible winglet 58
6.29 Drag coefficient as a function of AoA for rigid and flexible winglet 59
6.30 Load factor factor evolution with time for a gust of 11.5 ° 60
6.31 Lift coefficient as a function of AoA for rigid and actuated winglet 61
6.32 Load Factor as a function of AoA for rigid and actuated winglet 61
6.33 Drag coefficient as a function of AoA for rigid and actuated winglet 62

7.1 Gantt Diagram of the project 65

A.1 Lift in the wing as a function of the Cant Angle for a set of AoA 72
A.2 Lift in the winglet as a function of the Cant Angle for a set of AoA 73
A.3 Drag in the wing as a function of the Cant Angle for a set of AoA 74
A.4 Drag in the winglet as a function of the Cant Angle for a set of AoA 75

List of Tables

4.1 Grid independence study results 22
4.2 Geometric parameters of the wing and winglet 25
4.3 Parameters for the Aspect Ratio of the mesh 31
4.4 Parameters for the Skewness of the mesh 31

6.1 Characteristics of the aircraft for the gust calculations and the flight conditions 42
6.2 Summary of results for Maximum Aerodynamic efficency 49

7.1 Principal costs 63
7.2 Working Hours 63
7.3 Working prices 64
7.4 Final Budget 64

Chapter 1

Introduction

1.1 Motivation

Decreasing the fuel consumption as much as possible is one of the main challenges of modern aviation. The reasons of such an effort are the reduction in the aircraft emissions that harm the global warming as well as the money savings that this would produce. In order to reduce this fuel consumption, modern commercial aircraft have included in the last decades a type of wingtip devices called ”winglets”. As shown in Figure 1.1 winglets are a nearly vertical small-wing situated at an airplane’s wingtip that reduce Drag by inhibiting wingtip vortices.

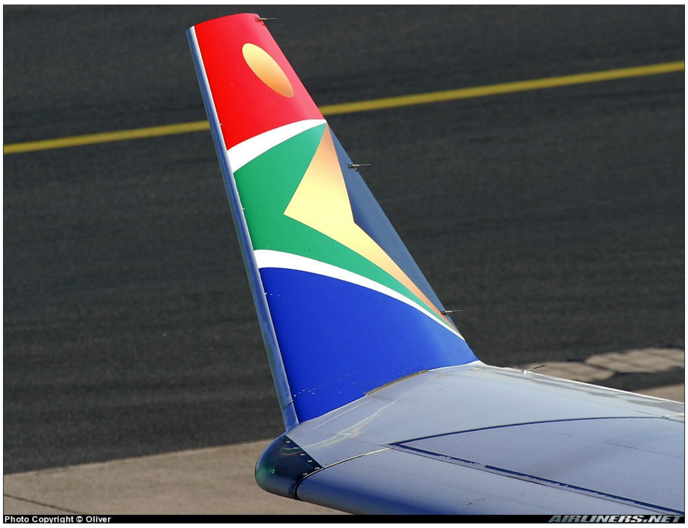

Figure 1.1: Winglet of an A330 aircraft.
By: `http://atwonline.com/aircraft-amp-engines/south-african-lease-six-a330-200s`

The improvements produced by current winglets designs consist on a reduction of Drag and a consequent increase in the Aerodynamic efficiency. Their principle of action consists on reducing the so-called induced Drag of the aircraft. This is the part of the Drag that appears due to the presence of Lift. The airplane generates Lift due to the difference in pressure between the upper and lower surface. This pressure difference creates the commonly named wingtip vortices, which increase the Drag of the aircraft. The effect ot these wingtip vortices is lowered due to the presence of winglets.

This bachelor thesis deals with the possibility of designing a new type of winglet which could diminish the ultimate gust loads, with the resulting reduction in aircraft weight. This diminution of the final gust load will be achieved by considering a flexible winglet that can adapt its position to the gust maneuver in order to optimize the loads that the aircraft suffers when it is subjected to this kind of turbulence.

1.2 Socio-economic frame

According to Airbus Global Market Forecast of 2015-2034 [1], aviation represents around a 4.1% of the total European GDP, concerning an approximate amount of 12 million jobs. The total aircraft departures reached 33 million worldwide in the year 2014, which supposed a 5% increase with respect to 2013. The load factors (in this case, refering to the amount of passengers per aircraft) of airlines are about an 80% and growing, which would be the same as seeing every car on the road with four of their five seats filled.

In this frame, the demands of airlines for new aircraft deliveries are expected to be a total amount of 32600 for new passenger aircraft and freighters between 2015 and 2034. This expected growth of aviation imposes the need of a new generation of "green" aircraft which reduce their emissions to the environment. Aircraft emissions are mainly due to the burn of Kerosene-Jet A or Jet A1- at the engines. When kerosene is burnt, it produces CO_2 and Nitrogen Oxides (NO_x), which are harmful for the atmosphere.

In fact, the present global trend to which aviation is headed is the maximum possible reduction of its environmental footprint. It has been reported [14] that the fuel burned nowadays is the half of the fuel burned in 1960. This tendency of fuel consumption decreasing over time is expected to continue in a future. In order to do so, the implementation of new aerodynamic designs is necessary, as well as more efficient systems, or a better management of the Global Air transport.

In this frame is in which initiatives like Clean Sky[1] (in the ACARE[2] frame) appear. Clean Sky is a Public Private Partnership between the European Commission and the European aeronautics industry whose main goals for the year 2020 are:

- 50 % reduction of CO_2 emissions through drastic reduction of fuel consumption.
- 80% reduction of NO_x (nitrogen oxide) emissions
- 50% reduction of external noise
- A green product life cycle: design, manufacturing, maintenance and disposal / recycling

The main objective of this project (as will be explained in section 1.7), is to create a winglet design that can decrease the weight of the airplane's wings. Such a new design type contributes to the Clean Sky goals of creating environment-friendly aircraft due to its potential fuel savings.

---

[1] `http://www.cleansky.eu/`

[2] `http://www.acare4europe.com/`

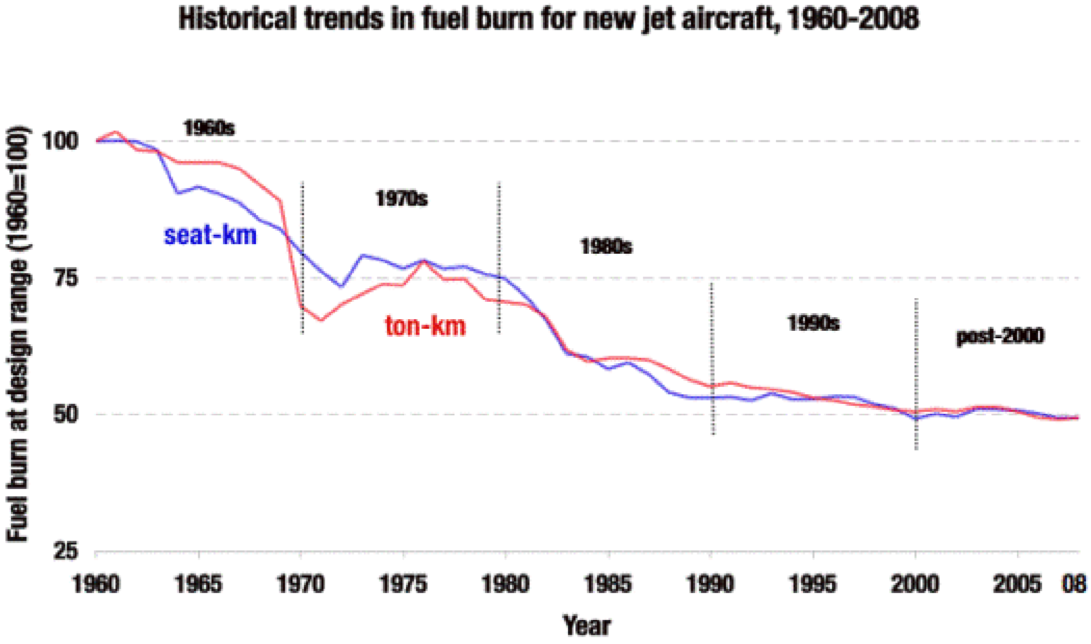

Figure 1.2: Evolution of the fuel consumption in history.
By: Rutherford, D., & Zeinali, M. (2009). *Efficiency Trends for New Commercial Jet Aircraft 1960 to 2008.*(`http://www.greenaironline.com/news.php?viewStory=684`)

Also, initiatives like SESAR[3], whose main objective is the better management of global Air transport with the consequent increase in Air Traffic capacity, try to diminish the impact of aviation in the environment. In order to achieve such objectives, new aircraft designs should be implemented.

1.3 Legal framework

EASA[4] (European Aviation Safety Agency) is an agency of the European Union which has regulatory and executive tasks over the civil aircraft. This agency together with the FAA[5] (Federal Aviation Administration), its American counterpart, are in charge of all the necessary regulations for the certification of civil aircraft on each territory. If an aircraft does not meet the standards proposed by each of them on each territory, it can not operate on it. The restrictions and guidance proposed by both organisms use to be the same so as to unify the supervision of aircraft on both regions. EASA sets its regulations in the so-called Certification Specifications (CS) while FAA does it on the Federal Aviation Regulations (FAR)

---

[3] `http://www.sesarju.eu/`
[4] `https://www.easa.europa.eu`
[5] `http://www.faa.gov/`

The present project deals with the abatement of wing loading during gusts, an atmospheric event that is described in section 1.4. The definition of a gust in aerospace industry is regulated by EASA and FAA. In particular, these regulations are stated in the EASA regulations CS-25, which are the regulations for large airplanes. Discrete gusts, are specified in the CS-25 [12], in the article CS 25.341, which specifies the *discrete Gust Design Criteria*. FAA sets the regulations for gusts in the FAR-25.341. All these regulations will be explained in detail on 1.4.1.

1.4 Gusts

As the aircraft flies, it encounters atmospheric turbulence. Turbulence is defined as small-scale, irregular air motions characterized by winds that vary in speed and direction and that is created by temperature differences. These variations in speed are normally considered on vertical, lateral and horizontal direction, however, in this thesis they will only be studied in the vertical orientation. Turbulence strongly affects the loads of the aircraft, and also can create discomfort or even injuries of the passengers. It can be divided into two main types of turbulence, which are Continuous turbulence, out of the scope of this thesis, and discrete gust. The present study will focus on discrete gust loads on the aircraft.

When an airplane encounters a gust, the vertical loads of the aircraft (Lift) increase according to the gust aggressiveness. This is the reason why gusts are important, since there are many parts of the aircraft whose ultimate loads are defined by means of them. The most important parts of the aircraft that are sized due to turbulence are:

- The wing
- The vertical tail plane
- The rear fuselage

1.4.1 Gust calculation

In the previously mentioned articles of EASA and FAA rules, the aircraft is assumed to be subjected to symmetrical vertical and lateral forces. For this study, only the vertical ones will be taken into account. According to this regulation, the shape of the gust has to be:

$$U = \frac{U_{ds}}{2}\left[1 - cos\left(\frac{\pi s}{H}\right)\right] \quad for \quad 0 \leq s \leq 2H \qquad\qquad U = 0 \quad for \quad s > 2H \tag{1.1}$$

In equation 1.1, s is the distance penetrated into the gust (in meters), U_{ds} is the design gust velocity in Equivalent air speed[6], and H is the gust gradient, which is the distance (meters) parallel to the aeroplane's flight path for the gust to reach its peak velocity. This distance will have a maximum in 350 ft and a minimum on 30 ft. The shape of these gusts can be seen in Figure 1.3.

---

[6] The equivalent air speed or EAS is a speed that would give the same dynamic pressure in sea level as the real dynamic pressure of the aircraft

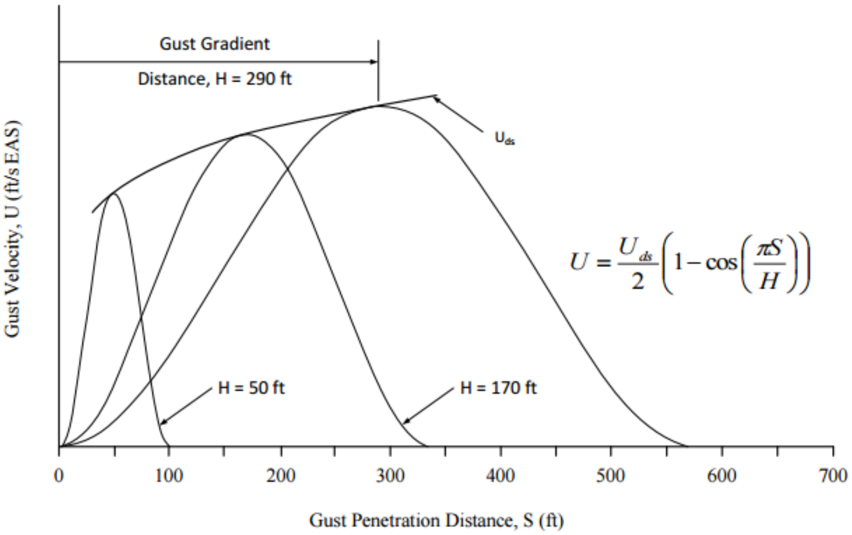

Figure 1.3: Typical (1-Cosine) Design Gust Velocity Profiles

The design velocity will be given by:

$$U_{ds} = U_{ref} F_g \left(H/350\right)^{1/6} \tag{1.2}$$

In equation 1.2, U_{ref} is the reference gust velocity in equivalent airspeed and F_g is the flight profile alleviation factor. It is important to notice that in this equation H has to bee in feet rather than in meter. The way in which this reference velocity has to vary with altitude for cruise speed is defined as follows in CS 25.341(a)[7]:

- At sea level it will have to be 17.07 (56.0 ft/s) m/s EAS.
- The reference gust velocity is reduced linearly from 17.07 m/s (56.0 ft/s) EAS at sea level to 13.41 m/s (44.0 ft/s) EAS at 4572 m (15 000 ft).
- The reference gust velocity is further reduced linearly from 13.41 m/s (44.0 ft/s) EAS at 4572 m (15 000 ft) to 6.36 m/s (20.86 ft/sec) EAS at 18288 m (60 000 ft).

The flight profile alleviation factor, F_g must be increased linearly from sea level value to a value of 1.0 at the maximum operating altitude. At sea level it is defined by:

$$F_{g0} = 0.5(F_{gz} + F_{gm}) \tag{1.3}$$

where :

$$F_{gz} = 1 - \frac{Z_{mo}}{76200} \tag{1.4}$$

$$F_{gm} = \sqrt{R_2 tan(\pi R_1/4)} \tag{1.5}$$

$$R_1 = \frac{MLW}{MTOW} \tag{1.6}$$

---

[7] `https://www.easa.europa.eu/certification-specifications/cs-25-large-aeroplanes`

$$R_2 = \frac{MZFW}{MTOW} \tag{1.7}$$

In these equations, Z_{mo} is the maximum operating altitude, MLW is the Maximum Lading Weight, MTOW is the Maximum Take-off Weight and MZFW is the Maximum Zero Fuel Weight.

The final equation for F_g will be given by:

$$F_g = F_{g0} + (1 - F_{g0})\frac{h}{Z_{mo}} \tag{1.8}$$

1.4.2 Main assumptions

The main assumptions for the rest of the project are:

1. In the present industry, the study of Discrete Tuned Gust (DTG) is performed by calculating the response of the aircraft to a gust under many altitude and gust situations. This means that the study is performed by sweeping many altitudes for a set of gust gradients (H). In this way, they can assess the performance of the aircraft under many situations, and study which is the most harmful one. Parametric studies of such magnitude are out of the scope of this thesis. The present study will be restricted to a fixed altitude and a unique gust gradient. In this case, the load mitigation for a particular case will be analysed.

2. Likewise, the vertical gust velocity will be assumed as a change in the Angle of Attack[8], so in order to study the gust situation, the difference between the gust and cruise will be an increase in this angle. This intensification of the Angle of Attack is what makes the Lift and Drag of the airplane grow, and then the loads are raised too.

3. It is known that when the Angle of Attack is suddenly increased, the increase in Lift is not instantaneous since it takes a time to reach its final value. This is expressed in the Wagner's function, which defines the variation in Lift with time when the Angle of Attack is increased by its half. The Wagner function represents the fraction of the final expected Lift as a function of the distance travelled in semi-chords, and can be seen in Figure 1.4.

---

[8] The Angle of Attack of an airfoil is the angle that the zero-thickness line of the airfoil forms with the forward component of the velocity

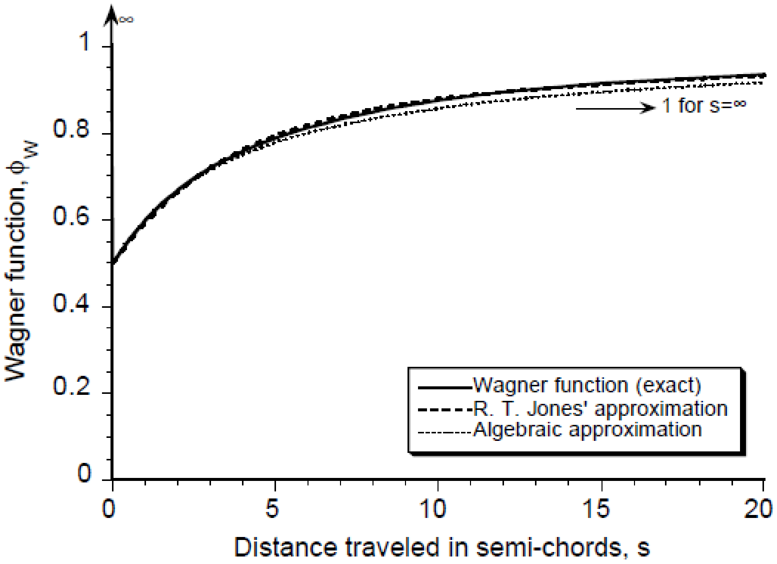

Figure 1.4: Wagner function representation
By: Leishman, J. G. (2002, January). *Challenges in modeling the unsteady aerodynamics of wind turbines*

In this study, this unsteadiness will not be considered, and then the Lift will be considered to change suddenly as the Angle of Attack does.

4. Also, when studying the dynamic response to gust, the reaction that the whole flying machine has when a (1-cos) gust appears may have importance under some situations. When the aircraft is subjected to these type of gusts, it also experiences a sudden relative change in altitude. This change in altitude alleviates the loads increase in a certain amount, by decreasing the Angle of Attack. Also, this effect will not be considered, which allows us to be conservative.

5. Finally, the aeroelastic effects that the gust have on the aircraft, such as the phase vibration created on the wingtip as well as wing twist, are out of the scope.

1.5 The proposed solution

In the present study, the performance of a wing with flexible winglets during a gust will be studied. As it has been explained, the loads that the aircraft experiences are intensified in the case of a gust. The main goal of the proposed solution is to decrease the loads that the aircraft suffers in the presence of this phenomenon.

The presented resolution, proposes a flexible winglet that can adapt its position according to the air stream so that the loads during gust are mitigated. The created alternative consists on a simplified structural model, in which the flexibility of a torsion spring between the wing and the winglet is modeled as an only function of the rigidity of this spring. Doing so, the winglet will modify its position for each flying condition, minimizing the loads that the airplane suffers in case of turbulence. This design is the passive design, inasmuch as it adapts its position passively.

Also, an alternative configuration will be considered for the proposed solution. In this arrangement, the winglet position can be actuated actively and then it can be selected depending on what is more convenient for each situation. This second procedure assimilates to what happens with flaps, spoilers and other active surfaces of the aircraft. This approach is the active design.

With these two approaches, the loads of the aircraft could be alleviated by varying the position of the winglet according to each flying status. This is important because, as explained before, the gust loads are those sizing some structures of the aircraft. If these loads can be mitigated, then the structure of the aircraft could reduce its weight so the fuel consumption will be decreased too. Also, the effects on Drag that this new design creates will be assessed.

1.6 Computational tool

In order to resolve the problem, the solver CFX of ANSYS will be used to simulate the aerodynamics of the selected wing. This solver is a tool based on Computational Fluid Dynamics (CFD). In all these simulations, the position of the winglet will vary in order to find which is the best position that it has to adopt for each situation. Later on, a detailed analysis of the data will be made in order to asses how should be the new design of the movable winglet.

1.7 Project objectives

The objectives of the project can be divided into one main objective and secondary objectives.

- **Main objective.** The main objective of this bachelor thesis is to evaluate the effect that the structural flexibility of a winglet has on aircraft loads for the case of a gust. For doing so, a simplified structural model in which a torsion spring is located between the wing and the winglet has to be proposed. In this model, the only variable will be the torsional stiffness of the torsion spring. With the created model, the position of the winglet will change as a function of the flight condition.

  In order to evaluate the effect of such a design in the aircraft loads, an aerodynamic model which solves the Navier Stokes equations with a commercial code(CFX) has to be formulated.

  The performance of the airplane has to be quantified for two flight conditions, which imply two load cases. The first one will be the cruise condition, in which the Lift of the aircraft is equal to its weight. The second one is the gust state, at which the aircraft loads are larger and then the performance with respect to cruise is different.

- **Secondary objectives.** There are some secondary objectives underlying the main objective which are summarized as:
  - CFX learning. In order to be able to perform a complete study in the CFX environment, it is necessary to have an initial overview of the program so that this tool can be managed.
  - Post-procesing of results. The results obtained with the aerodynamic model have to be post-processed so as to obtain the load assuagement produced by the suggested solution.
  - Actuated winglet. Apart from the reduction in loads produced by a flexible winglet, the same approach has to be calculated for the case of an actuated one. This additional design approach should be also beneficial for the airplane structure.

1.8 Document overview

- Chapter 2 introduces the state of the art in winglet designs, wing morphing and active control of aerodynamic loads during gust conditions.
- Chapter 3 explains the characteristics of the software used for all the aerodynamic computations. It illustrates all the benefits of this software among others.
- Chapter 4 summarizes all the information relative to the final geometry and mesh, including a grid independence study.
- Chapter 5 reviews all the mathematical procedures followed after running all the simulations.
- Chapter 6 contains all the final results
- Chapter 7 encloses the budget and the planning of the project.
- Finally, Chapter 8 provides the project's conclusions and future work.

Chapter 2

State of the art

2.1 Winglets and movable wingtips

There are many types of wingtip devices that have been used on airplane. They can be found in [2] and [3]. Some of these are: Winglet, Blended winglet, Up-down winglet, Wingtip fence, Raked wingtip and Spiroid tipped wing. The considered wingtip device for this study will be the winglet. All these types of wingtips are seen in Figure 2.1.

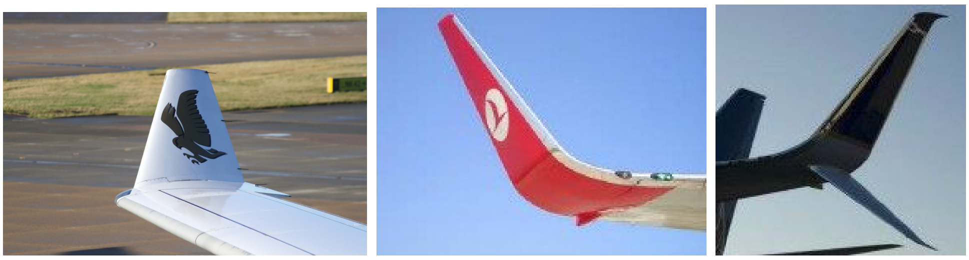

(a) Winglet. By: `https://www.flickr.com/photos/mals_r/8471335777`

(b) Blended winglet. By: `http://flitetest.com/articles/why-do-planes-have-winglets`

(c) Up-down winglet. By: `http://flitetest.com/articles/why-do-planes-have-winglets`

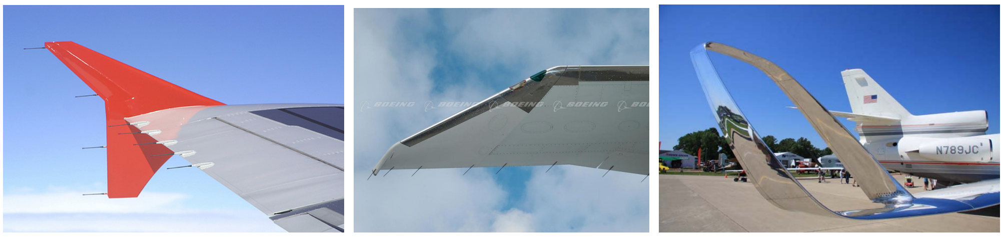

(d) Wingtip fence. By: `http://www.flickriver.com/photos/tags/wingtipfence/interesting/`

(e) Raked wingtip. By: `http://www.boeingimages.com/`

(f) Spiroid tipped wing. By `https://es.pinterest.com/ahmadh_89/aircraft-winglet-design/`

Figure 2.1: Types of wingtip devices

Relating aircraft with variable winglet position, there are some studies that assess the working capabilities of the aircraft for different Cant Angles. The Cant Angle is the angle that the winglet forms with the horizontal line of the wing. There are many articles that study the effect of changing the Cant Angle in order to optimize the performance of the wing. [4] analyses the performance of a wing at different Cant Angles. It concludes that in order to reduce the fuel consumption of airliners, the position of the winglet should imply low Cant Angles at low Angles of Attack and relatively high Cant Angles at high Angles of Attack. In this way, the winglet would be optimal for each flight condition. [5] also studies the differences between different Cant Angle. In this paper, the Cant Angle is called to the angle that the winglet forms with the vertical, instead of the angle with the horizontal, as it is commonly noted. In this study, it is proved that all wing with winglets have higher aerodynamic efficiency than wings without them. In this model, the Cant Angle for lowest Drag is found to be 45°.

It is of relative importance [6] and [7]. Both studies assess the performance of an aircraft in gust when the win-tip moves passively with air. This design, alleviates the loads that the airplane suffers in case of gusts. The proposed design, which is similar for both, can be seen in Figure 2.2. In the proposed designs, the wingtip would move upwards as the wing increases its Angle of Attack, and then it would reduce the loads under gust conditions. In these publications it is estimated that the reduction in the bending moment produced by this wingtip design is of about a 18 %. However, these studies are more focused on the structural and dynamic standpoint of this design instead of on the total final aerodynamic loads. This model and the one proposed here will differ on the position of the spring, which is different between both, since in the proposed model the torsion spring is at the hinge between the wing and the winglet. Then, the proposed model will study the movement of the wingtip in the bending direction rather than in the pitching one.

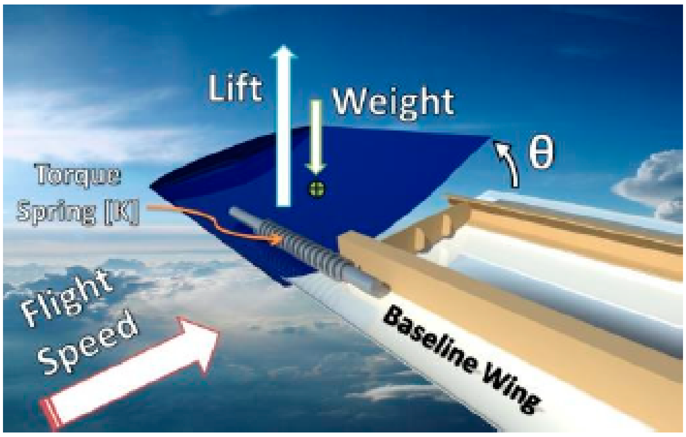

Figure 2.2: Passive wingtip dessign
By: Guo, S., Los Monteros, D., Espinosa, J., & Liu, Y. (2015). *Gust Alleviation of a Large Aircraft with a Passive Twist Wingtip.*

In [8] it is proposed a wingtip device called MORPHLET[1]. In this study, it is assessed the possibility of changing the position of the winglet of an airplane depending on the type of cruising conditions. This position would differ in different conditions like initial cruise phase or final phase. In this publication, it is estimated that varying the winglet position for these two different cruise conditions may have beneficial effects in the reduction of Drag and the consequent increase in Range. The shape that this winglet can adopt is more complex than just a change in the Cant Angle, since it acquires many different forms different from varying he Cant Angle.

---

[1] This comes from the acronym of MORphing wingLET

[9] analyzes the possibility of using a winglet with variable Cant Angle in order to control the movement of the airplane, substituting in this way control surfaces like ailerons, elevators and rudders.

The company Tamarack Aerospace created what they call the ATLAS (Active Technology Load Alleviation System). With this system, they propose an active winglet which can alleviate the loads in maneuvers like gust, without compromising the control maneuvers as happens actually in airplanes like 787 or A320 which use ailerons or spoilers to do so. This system has been certified in Europe for the CJ, CJ1 and CJ1+ aircraft. FAA certification is expected to be finally true on summer 2016. This active winglet system has been installed in April 29th, 2016 in a Cessna Citation CJ aircraft HB-VPF operated by private hire company JetPingu.

2.2 Morphing wings

By directly comparing aircraft with nature, designers seek inspiration, in order to achieve the simplicity, elegance, and efficiency that characterize animal species obtained by thousands of years of biological evolution. Even in complex urban environments, birds are able to rapidly change shape to transition from efficient cruise to aggressive maneuvering and precision descents. In order to imitate nature, aerodynamicists and structure designers try to create the so-called Morphing-wing aircraft. These aircraft adapt the shape or their wings in order to adapt the airplane to each flying condition, providing in this way a more-optimal performance.

[10] provides a review of all the benefits of Morphing wings. The timeline of aircraft using morphing technologies of this publication can be seen in Figure 2.3. It highlights that since first aircraft designs, the idea of morphing has been present. However, it has always led to penalties in terms of cost, complexity or weight increase. This publication categorizes the geometrical parameters that can be affected by morphing into: planform alteration , out-of plane transformation , and airfoil adjustment. Out of this division, the considered winglet geometry will be into the out-of plane transformation as well as a change in the wing diedral.

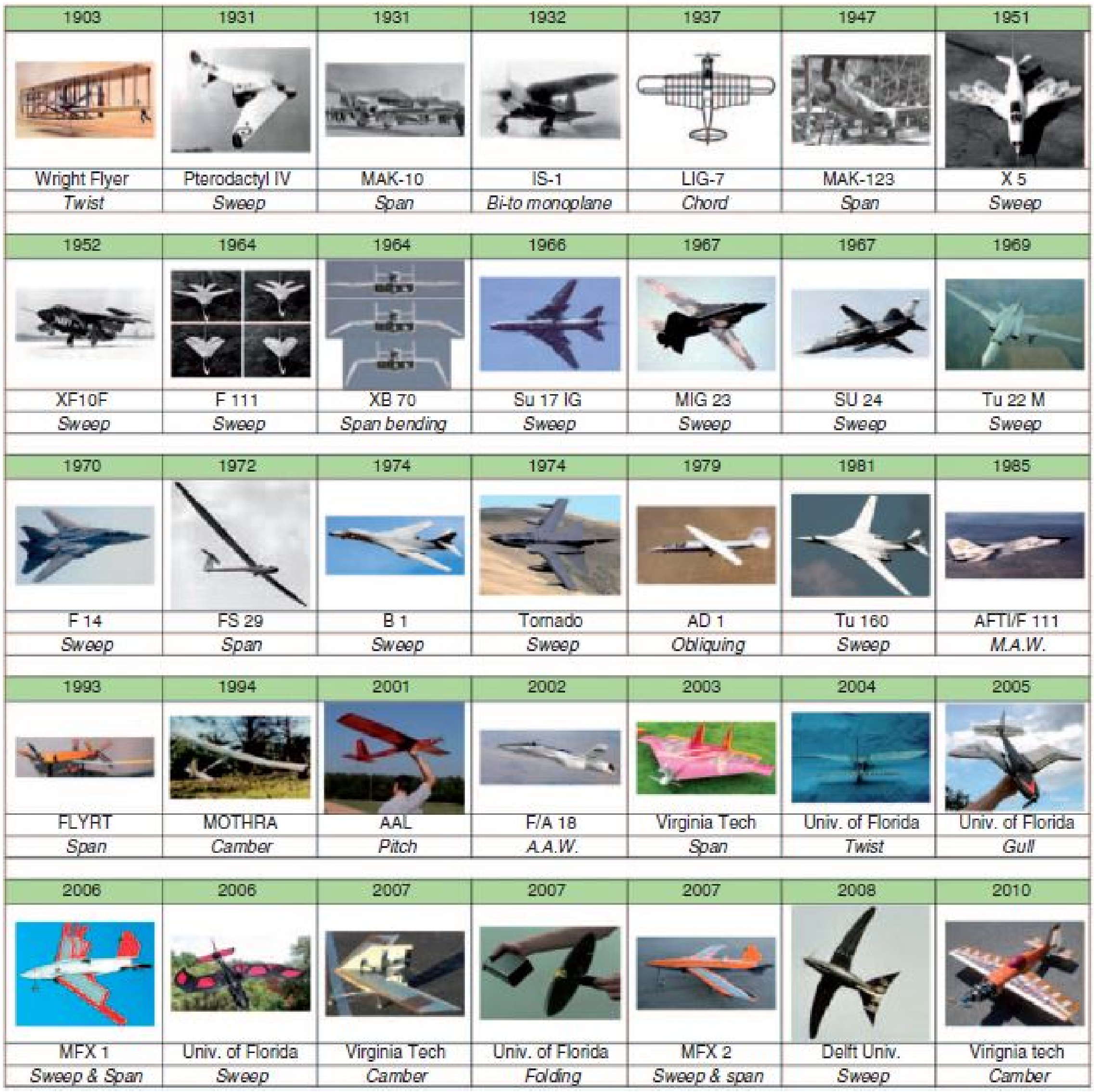

1903	1931	1931	1932	1937	1947	1951
Wright Flyer	Pterodactyl IV	MAK-10	IS-1	LIG-7	MAK-123	X 5
Twist	*Sweep*	*Span*	*Bi-to monoplane*	*Chord*	*Span*	*Sweep*
1952	1964	1964	1966	1967	1967	1969
XF10F	F 111	XB 70	Su 17 IG	MIG 23	SU 24	Tu 22 M
Sweep	*Sweep*	*Span bending*	*Sweep*	*Sweep*	*Sweep*	*Sweep*
1970	1972	1974	1974	1979	1981	1985
F 14	FS 29	B 1	Tornado	AD 1	Tu 160	AFTI/F 111
Sweep	*Span*	*Sweep*	*Sweep*	*Obliquing*	*Sweep*	*M.A.W.*
1993	1994	2001	2002	2003	2004	2005
FLYRT	MOTHRA	AAL	F/A 18	Virginia Tech	Univ. of Florida	Univ. of Florida
Span	*Camber*	*Pitch*	*A.A.W.*	*Span*	*Twist*	*Gull*
2006	2006	2007	2007	2007	2008	2010
MFX 1	Univ. of Florida	Virginia Tech	Univ. of Florida	MFX 2	Delft Univ.	Virignia tech
Sweep & Span	*Sweep*	*Camber*	*Folding*	*Sweep & span*	*Sweep*	*Camber*

Figure 2.3: Timeline of aircraft using morphing technology
By: Barbarino, S., Bilgen, O., Ajaj, R. M., Friswell, M. I., & Inman, D. J. (2011). *A review of morphing aircraft.*

Chapter 3

ANSYS CFX solver

CFX is a Computational Fluid Dynamics (CFD) solver. It is a computer-based tool for simulating the behaviour of systems involving fluid flow, heat transfer and other related physical processes. It is integrated in the ANSYS Workbench, which also has programs to calculate structural or mechanical problems. It works by solving the Navier-Stokes equations, which are the classical fluid-dynamics differential equations solving momentum, heat and mass transfer. These equations can be solved numerically, and so does CFX.

CFX uses a a finite volume formulation to numerically solve the Navier-Stokes equations. In this type of formulation, the region of interest (which depends on the problem type) is divided into regions called control-volumes. These control volumes are commonly refered to as the mesh. The equations are discretized and solved in each control volume using an iterative algorithm. Later on, an approximation of the value of each variable (density, pressure, temperature) at specific points through the domain can be obtained by interpolation. CFX is cell-vertex finite volume, coupled implicit, pressure based solution technique (i.e., solves for pressure and velocity at the same time). In vertex based schemes the flow variables are stored at the vertices of the mesh elements. This differs to cell-centered schemes in which the variables are stored in the center of the elements.

In order to do this, a domain in which the equations are to be solved is created. This domain will be as large as possible in order to approximate the fluid region reasonably to reality.

3.1 Advantages of CFX for the aeronautic industry

CFX is a leading and established general purpose CFD code for internal and external aerodynamic fluid flow analyses that can be used for all of these applications. Examples where CFD is being used in the aeronautics industry are the prediction of Lift and Drag of airfoils and wings, flow around fuselages and entire aircrafts. In the aeronautics industry there are several key demands on a modern CFD tool which the CFX software addresses. The main reason why CFX was selected among other software for the present project is because it is the preferred CFD package by AIRBUS Group for the aerodynamic computations. The following characteristics make it better than other CFD softwares for this industry:

- **Geometry.** The pre-processor CFX-Build allows the user to generate the geometry from scratch using tools such as projection or extrusion. In addition, it allows the user to import the geometry files from programs like CATIA, which is greatly used in the aeronautical industry.

- **Mesh generation.** It provides a really high geometric flexibility, yielding to a complete developed algorithm for creating unstructured meshes.
- **User-friendly handling.** A complete Graphical User Interface driven definition of the case and appropriate pre-processing (CFX-Build) and post-processing (CFX-Post) tools for setting up the simulation and for qualitative and quantitative analyses of the results allows the engineer to focus on the analysis of the device rather than on the needed settings.
- **Advanced turbulence models.** In order to obtain accurate solutions it is essential to use advanced turbulence models, which reproduce the physics of turbulence. CFX provides the user a complete set of turbulence models. For more information about all of them see [19].
- **Robust and fast numerical solution methods.** CFX solver technology employs a unique and leading combination of robust and accurate higher-order numerical discretization schemes, algebraic multi-grid solution method and scalable parallel computing on homogeneous and heterogeneous computer platforms.
- **Advanced integration into design environments.** Interactive modification of run time parameters and batch programming capabilities allows to use CFX for optimisation of engineering devices. Fluid properties, boundary conditions, solution parameters, and job control are accessible through parameter files.

3.2 Turbulence modeling

Turbulence is an unsteady, irregular and chaotic movement of the flow that uses to happen at large Reynolds numbers, when inertia forces in the fluid become significant compared to viscous forces. It would be incorrect to say that it is a random movement since turbulence is governed by Navier-Stokes equations. In ANSYS CFX solver, there are many turbulence RANS (Reynolds Averaged N-S) models that can be selected in order to solve the Navier-Stokes equations when then flow is turbulent.

RANS models decompose the instantaneous variables (for example the velocity components and the pressure) into a mean value and a fluctuating value and it is expressed in the form:

$$u_i = \bar{u}_i + u'_i \tag{3.1}$$

The Navier-Stokes equation of momentum is given by:

$$\rho\partial_t u_i + \rho u_j \partial_j u_i = -\partial_i p + \partial_j \bar{\bar{\tau}}'_{i,j} \tag{3.2}$$

After applying equation 3.1 to the momentum equation, it is found that[1]:

$$\rho\partial_t \bar{u}_i + \rho\bar{u}_j \partial_j \bar{u}_i = -\partial_i \bar{p} + \partial_j \bar{\bar{\tau}}'_{i,j} - \partial_j \rho\overline{u'_i u'_j}. \tag{3.3}$$

---

[1] For simplicity in the explanation, it is written the incompressible equation. However, CFX has the option of solving the compressible ones.

where the subindex ”i” indicates the component of the momentum equation, (x,y, and z) and the Einstein convention applies to the repeated inde ”j” [2].

The most important term in this equation for the RANS models is $-\rho\overline{u_i'u_j'}$, which is called Reynolds Stresses. Each RANS model expresses the Reynolds stresses as a function of the mean velocity instead of the fluctuation in a different way. Within all those, the selected one is *Eddy viscosity transport.* This model assumes that the Reynold Stresses are proportional to mean velocity gradients. Eddy viscosity models can be of three types: 0 equations, 1 equation or 2 equations models. The three models are named depending on the additional number of partial differential equations that are being solved. Out of these three types the used one is the 1-equation Spalart-Allmaras model [11]. This model expresses the Reynolds stresses as function of the so-called turbulent or eddy viscosity ν_T, which depends on the flow and is not homogeneous.

---

[2] For instance, $\bar{u}_j \partial_j \bar{u}_i$ in the x-direction would be $U_x \dfrac{\partial u_x}{dx} + U_y \dfrac{\partial u_x}{dy} + U_z \dfrac{\partial u_x}{dz}$.

Chapter 4

Geometry and Mesh

In this chapter, the preliminary grid independence study is presented. Also, the geometry of the wing under study is proposed to the reader. Besides, the geometry of the 3D domain created for all the simulations is detailed. Finally, the mesh associated to this geometry with its specifications and statistics is offered.

4.1 Grid independence study

The grid independence study is a parametric study performed to a mesh so as to know how it has to be sized. In this section, a grid independence study is performed to a 2D airfoil, similar as the airfoil of the considered wing. The purpose of this study is to know the needed discretization that has to be selected for the airfoil so that we are precise enough to represent the problem without loosing accuracy. When working with computational fluid dynamics, as explained before, the geometry has to be discretized into small subdomains. This analysis is made in order to optimize as much as possible the grid under consideration, reducing in this way the number of elements and nodes. In order to do so, the evaluated parameter will be the number of divisions in which the airfoil is discretized [1]. The number of divisions will be adjusted between 150 and 750 so as to know how the final results differ as the discretization changes. It is important to notice that the number of divisions in which the airfoil is discretized are the divisions of the whole airfoil, so in the 150 divisions case, the upper surface will have 75 sections, and so will have the lower.

A 2D analysis of an airfoil is the study of a section of an ideally infinite wing. This cannot be performed in the CFX domain since it does not read 2D geometries. Then, in order to do so, the analysis of the airfoil is performed to a very thin section (the selected thickness is 0.01 m) so that is is very similar to a 2D case.

4.1.1 CFX settings

The airfoil under study for the whole project (grid independence study and 3D analysis) will be a NACA 65_3218. The selected Angle of Attack for the grid independence study is 5^o. The airspeed of the free-stream is 87.5 m/s. The properties of the air are:

- $\rho = 1.19\ kg/m^3$
- $\mu = 1.825 \times 10^{-5}\ kg/m \cdot s$

---

[1] Notice that the ideal number of divisions would be infinite, but since this is not possible, this parameter has to be selected

- $T = 25°C$
- $P = 101325 \quad Pa$

The computational fluid domain for the simulations is a C-meshed domain, as sketched in Figure 4.1. There is a smaller subdomain around the airfoil, where the mesh resolution is higher (smaller elements). This is due to the fact that in the region that is close to the airfoil, the pressure and velocity contours change widely, and then a finer mesh is needed. Also, an inflation layer is created around the airfoil for calculating the turbulent region over it.

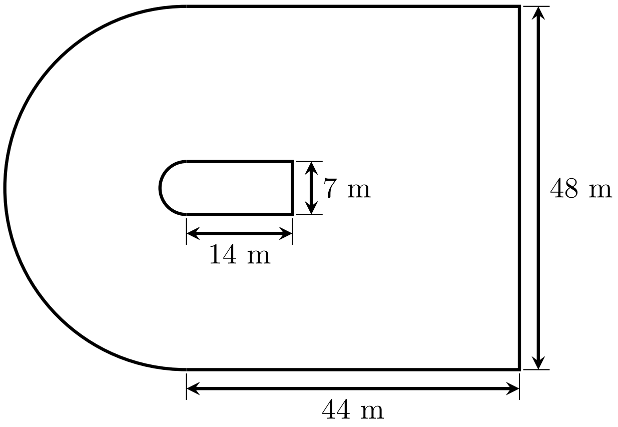

Figure 4.1: Sketch of the mesh domains

The characteristics of the mesh under study are:

- The finner subdomain in which the mesh is refined has elements with mean-size[2] of 0.1 m.
- The coarser domain has elements with a mean-size of 0.8 m.
- The inflation layer surrounding the airfoil has 10 layers, with an initial height of 0.0008 m and a growing rate of 1.2.

These parameters are fixed in each considered case, and the only parameter varying is the number of divisions of the airfoil.

---

[2] The mean-size of the sub-domains is the average of the sides of each element

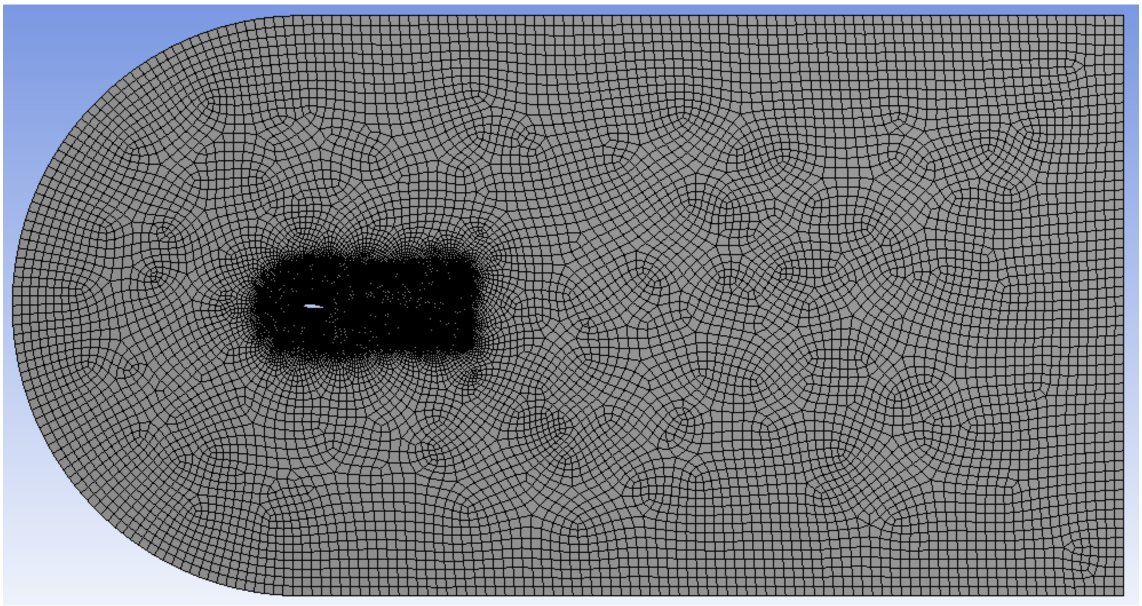

Figure 4.2: Final mesh for the grid independence study

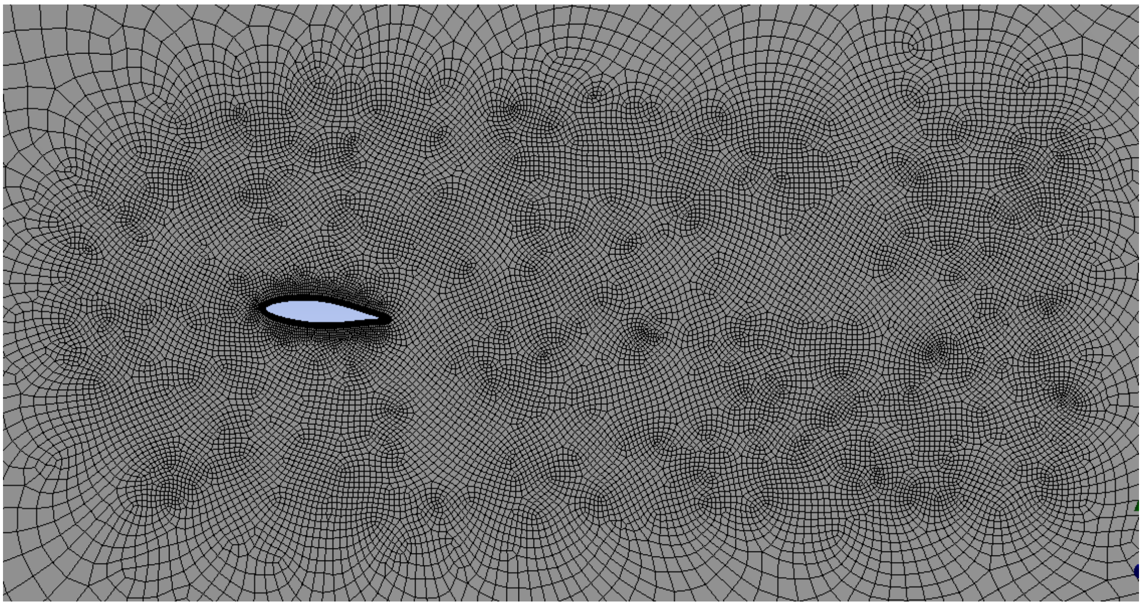

Figure 4.3: Detail of the mesh close to the airfoil

4.1.2 Simulations information

When running a simulation with CFX, some parameters have to be selected so that the iteration that it performs converges well. It has to be selected an initial condition for all the variables. For this, the default initial condition set by ANSYS is selected since it is good enough for this purpose. For more information relative to the CFX initial conditions see [20], chapter 3 . This initial condition selection will be maintained through all the simulations run in this project. Besides, the boundary conditions for all the surfaces on the mesh have to be chosen. The boundary conditions for the grid independence study are:

- A symmetry boundary condition is selected on each of the lateral faces of the mesh so that the simulation emulates an infinite wing geometry.
- The boundary condition on the airfoil is non-slip wall.
- Inlet and outlet are specified with a pressure-inlet/outlet boundary condition.
- Upper and lower surfaces have free-slip wall boundary condition

For more information relating the characteristics of each boundary condition go to [20], chapter 2. Also, the convergence point of each simulation has to be chosen. In general terms, it is considered that a simulation has converged when the residuals of the simulation (see [23]) stop changing. This is the selection for the grid independence study. When the residuals do not vary anymore with each iteration, the simulation will stop.

4.1.3 Grid independence study results

Once all the information relative to the mesh and simulation settings has been stated, table 4.1 summarizes all the obtained results. The parameters in which the study is going to be made are the Lift, the Drag, and the Pitching moment. By loooking at the different values for these parameters, it is going to be seen how them fluctuate as the number of divisions of the airfoil changes.

Number of divisions	Lift (N)	error %	Drag (N)	error %	Pitch (N.m)	error %
150	72.211	2.79	1.2451	5.11	48.459	3.94
250	71.458	1.71	1.2262	3.52	47.781	2.48
300	71.309	1.50	1.204	1.64	47.602	2.10
500	70.486	0.33	1.1948	0.869	46.885	0.56
750 [1]	70.25	-	1.1845	-	46.622	-

Table 4.1: Grid independence study results

With these results, **the resolution for the rest of the project is set to 150 points per chord (75 in the upper surface and other 75 in the lower)**. This is due to the fact that the maximum error, which appears to be on the Drag, is a 5.11 %, which is a reasonable error margin for the purpose of the present analysis.

4.1.4 Validation of the mesh

In order to validate the selected mesh parameters for the inflation layer and airfoil sizing, the validity of the mesh at the boundary layer of the airfoil has to be checked. This is due to the fact that when the boundary layer is turbulent, it is divided into two regions, one inner region with a thickness about 10-20% of the entire boundary layer, and one outer region. The velocity gradients in all the boundary layer are large (the inner part has a linear velocity profile while the outer has a logarithmic profile) and have to be accounted. This is why the inflation layer is created, so as to report these changes in velocity.

---

[1] Notice that for the study, the airfoil with 750 divisions is considered to be the solution, with respect to which the error is to be considered. This is due to the fact that the divisions are very small as compared to the airfoil chord for it to be considered a very accurate solution (of the order of 1 mm while the airfoil is 2 m)

The validation of the inflation layer and airfoil sizing is performed in terms of the dimensionless variable y^+. This parameter is related to the velocity of the boundary layer and is used to check the validity of the selected turbulence model. For more information regarding y^+ and the distribution of velocities of the boundary layer see [15] and [19].

For assessing the validity of the results, ANSYS software states the necessary values of y^+ over a surface for it to be valid. The upper limit for y^+ is 300, while the lowest is 11.06. In the cases where y^+ is bellow this number, ANSYS automatically sets the value of y^+ to 11.06 to avoid mesh inconsistencies.

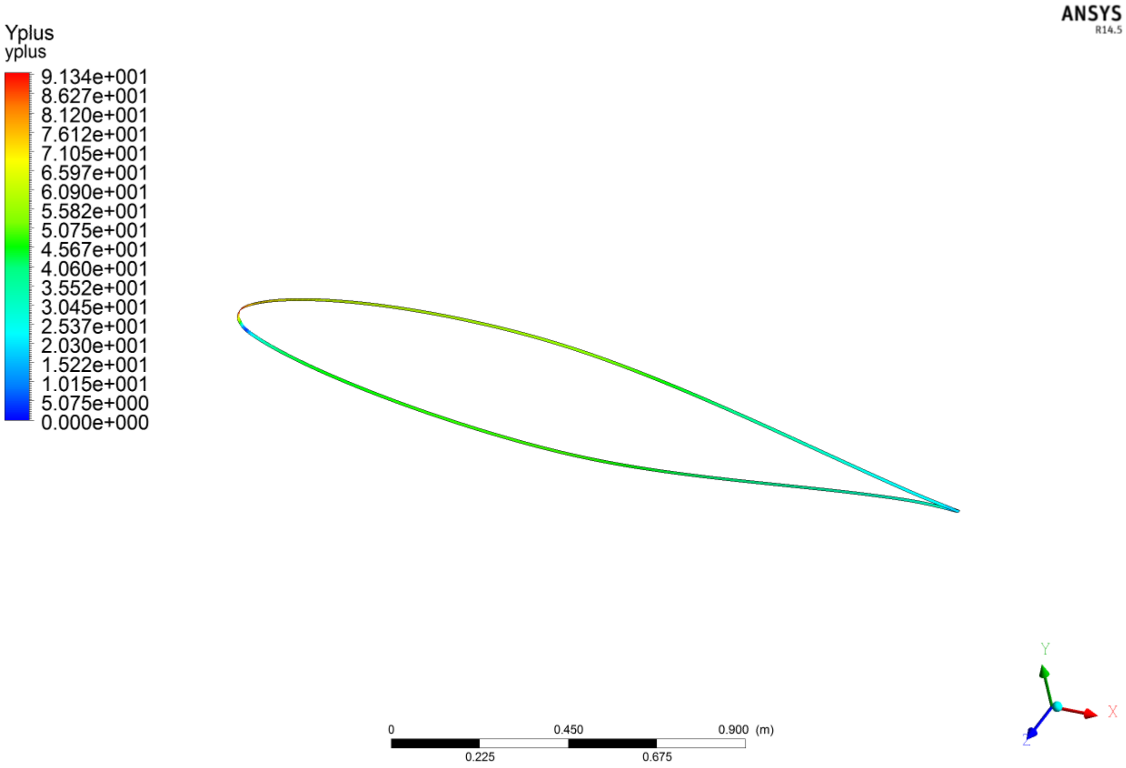

Figure 4.4: Values of y^+ along the airfoil

Figure 4.4 shows the values of y^+ over the airfoil for the simulation with 150 divisions. In this Figure, it can be seen how the majority of the points in the airfoil have values that are higher than 11.06. There are some points in which it is lower. This is due to the presence of stagnation points on the airfoil, which will always have $y^+ = 0$. Also, it can be seen how the upper limit for y^+ in the airfoil is pretty much below the maximum one. In this way, the mesh is validated.

4.2 Geometry

In this section, the geometry of the studied wing is presented.

4.2.1 Geometry definition

The wing that is used for the whole study will be one similar to the one of the C-212 Aviocar. The span of the wing is 21 m. The airfoil, as explained before, is a NACA 65_3218, that does have a chord of 2 meters from the root to a span of 5 m. Aft, the wing has a taper ratio of 0.5. All this information is summarized in Figure 4.5.

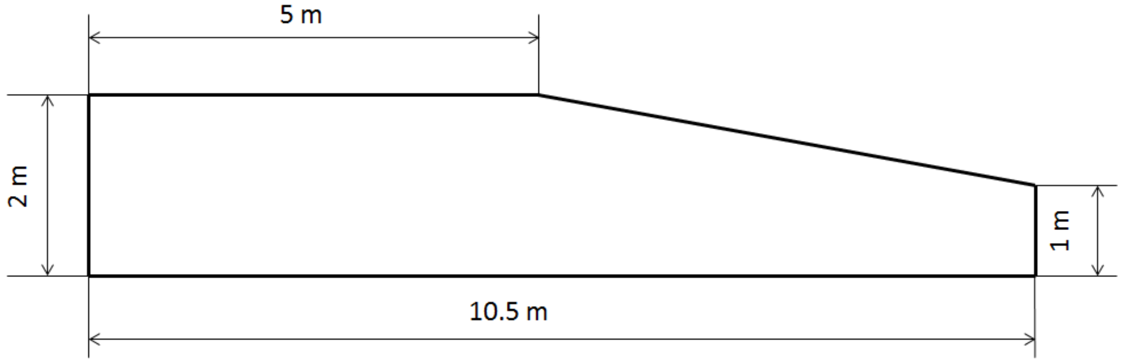

Figure 4.5: Schematic of the wing planform without winglet

The winglet, that is placed at the tip of the wing, sweeps its chord from 1 m at its root to 0.5 m at the tip, being 1 m long. The sketch for the winglet planform can be seen in Figure 4.6.

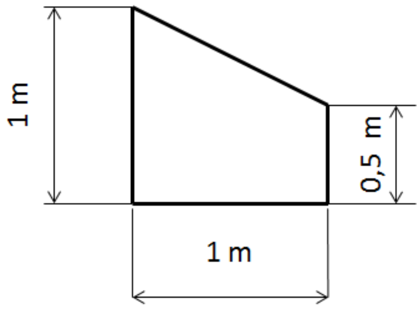

Figure 4.6: Schematic of the winglet planform

The angle that the winglet forms with the wing is the so-called Cant Angle[3]. It will be varied with respect to the mean center-line of the wing, and will be denoted as θ_w, as can be seen in Figure 4.7. The final geometry of the created wing+winglet geometry on the CFX domain is seen in Figure 4.8.

---

[3] In some Literature, the Cant Angle is called to the angle between the vertical line and the winglet instead of the horizontal

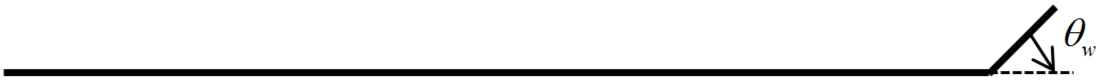

Figure 4.7: Schematic of the winglet angle with respect to the mean line of the wing

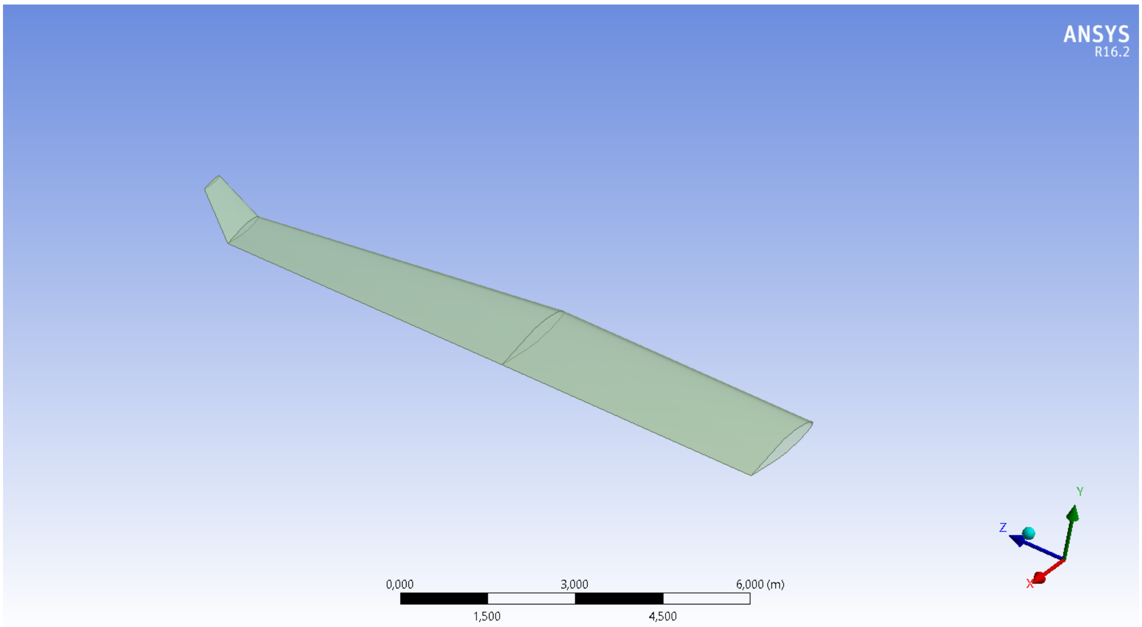

Figure 4.8: Final Wing and winglet in ANSYS workbench for a winglet angle of 50 º

4.2.2 Geometric parameters

When talking about wings, there are many parameters that have to be calculated in order to know its performance. In order to do this, the parameters for the wing and winglet will be calculated as if they were two separated wings.

	Wing	Winglet(isolated)
Surface (S) $[m^2]$	36.5	0.75
Mean Aerodynamic Chord(MAC) [m]	1.7991	0.7777
MAC position(y_{MAC}) [m]	4.735	0.444
Aspect ratio (AR)	12.082	1.333

Table 4.2: Geometric parameters of the wing and winglet

The formulation for these parameters is:

$$S = bc_{root}\frac{1+\lambda}{2} \tag{4.1}$$

In equation 4.1, b is the span of the wing, c_{root} is the chord at the root and λ is the taper ratio (c_{tip}/c_{root}). Notice that if different sections have different taper ratio, as is the case, the parameters have to be computed separately.

$$MAC = \frac{2}{3} c_{root} \frac{1 + \lambda + \lambda^2}{1 + \lambda} \tag{4.2}$$

$$y_{MAC} = \frac{b}{6} \frac{1 + 2\lambda}{1 + \lambda} \tag{4.3}$$

$$AR = \frac{b^2}{S} \tag{4.4}$$

4.3 Mesh

4.3.1 Mesh domain

The domain of the mesh will be an extrusion of that one used in the 2D simulations for the grid independence study (see Figure 4.1). In this case, the study will be performed in the half of the wing, imposing a symmetry boundary condition in the wall which coincides with the root in order to save computing time. The extrusion will have a width of 3 times the semi-span of the wing. The refined region will be extruded the same length as the wing+winglet is, adding a margin at the tip of the winglet. All this can be seen in Figure 4.9.

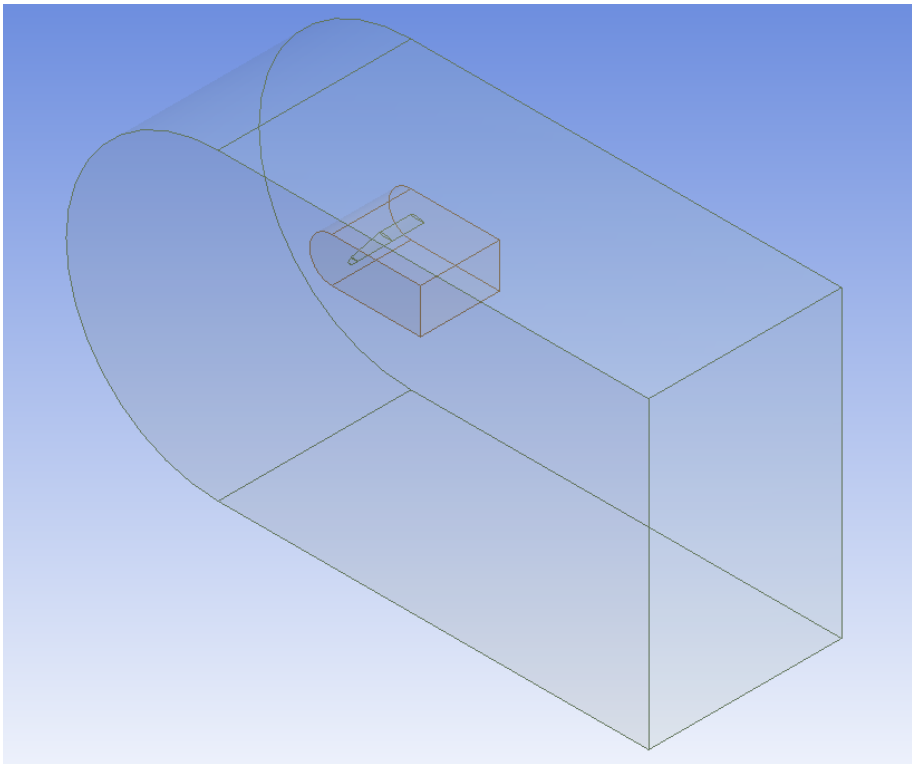

Figure 4.9: Mesh domains

4.3.2 Mesh characteristics

The following charateristics define the mesh in the proposed domain:

- The sizing in the face of the wing is set to be 0.026 m. The reason is because of the selection of the number of elements through the grid independence study. The number of elements selected in the whole airfoil is 150. Then, each part of the airfoil (upper ad lower) will have 75 elements. If the chord is divided by the number of elements, it is obtained 2/75=0.026, which is selected to be the sizing of this face. Following a similar procedure, the sizing for the winglet face is selected in 0.013 m, since the chord at its root is 1 m.
- The inner body in which the mesh is refined has elements with size of 0.3 m.
- The bigger domain has elements with a size of 2.5 m.
- The inflation layer surrounding the wing and winglet has 10 layers, with an initial height of 0.0008 m and a growing rate of 1.2.

In order to optimize the mesh, the sizing for the two subdomains is changed with respect to the sizing of the grid independence study. This is because when performing the 3D mesh, it was seen that, by maintaining these numbers, the number of elements was too large and the computing time was humongous. The sizing of the wing and winglet faces as well as the boundary layer have been maintained, since the goal of the grid independence study was to infer the needed airfoil sizing. The final mesh created for the 3D case are seen in Figures 4.10, 4.11, 4.12, 4.13, 4.14 and 4.15. On them, there can be seen some surfaces in which the boundary conditions have to be set. The boundary conditions on these surfaces are:

- The wing and winglet Boundary condition is a non-slip wall.
- The boundary condition for the upper, lower and exterior surface are is free-slip wall.
- The boundary condition of the plane of symmetry is a symmetry boundary condition.
- The inlet and the outlet have a boundary condition of pressure-inlet/outlet

As illustrated in chapter 4.1, for information relative to the boundary conditions of CFX see [20], chapter 2.

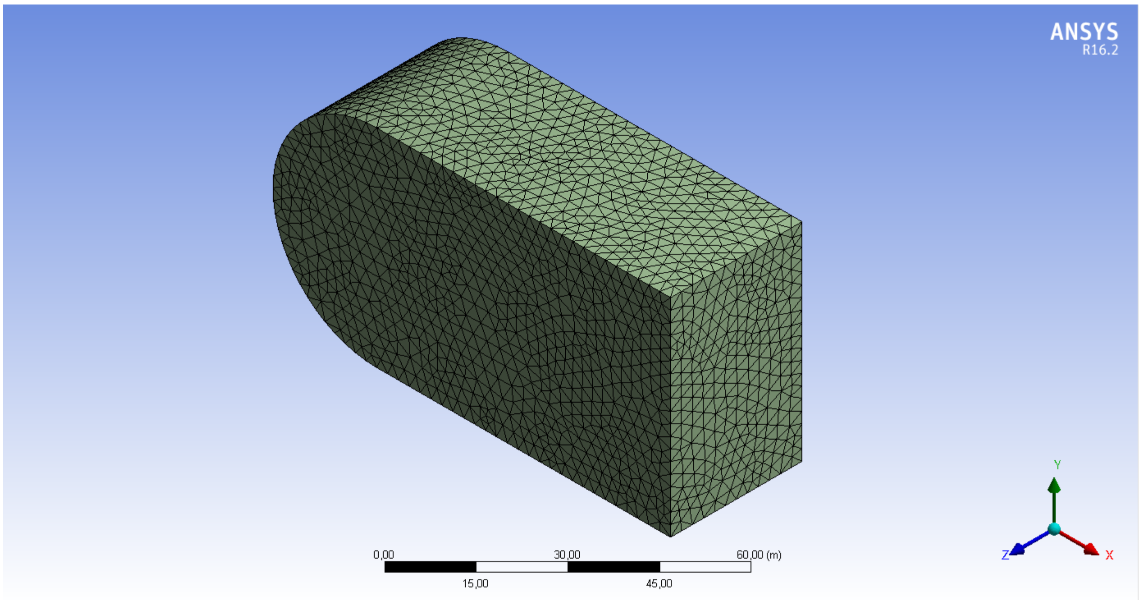
ANSYS
R16.2
0,00
30,00
60,00 (m)
15,00
45,00
Y
Z
X

Figure 4.10: Final Mesh

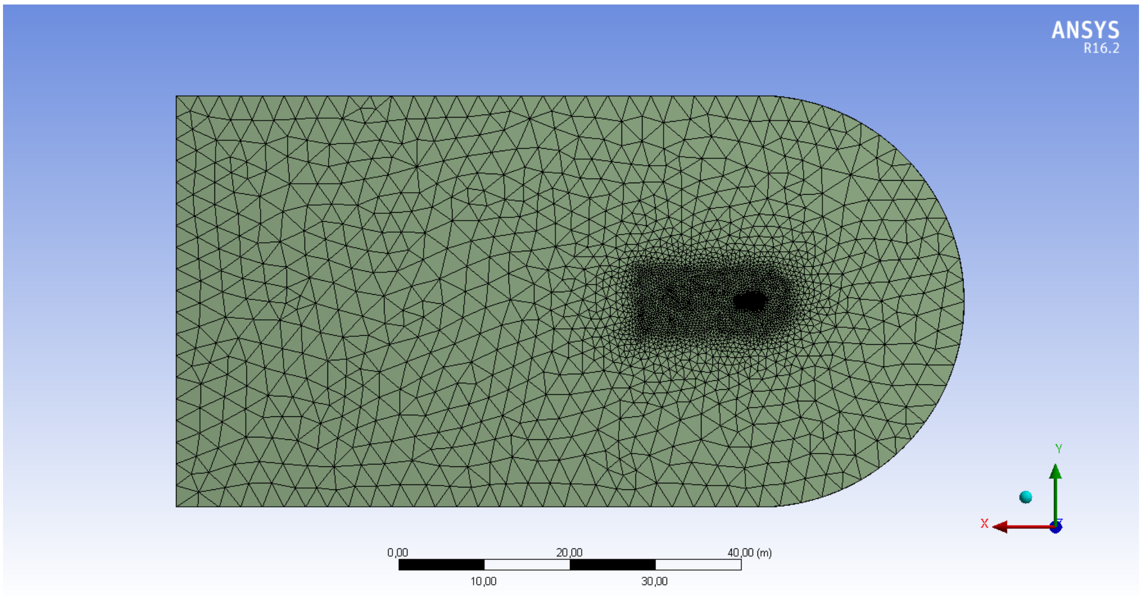
ANSYS
R16.2
0,00
20,00
40,00 (m)
10,00
30,00
Y
X

Figure 4.11: Final mesh focused on the symmetry plane

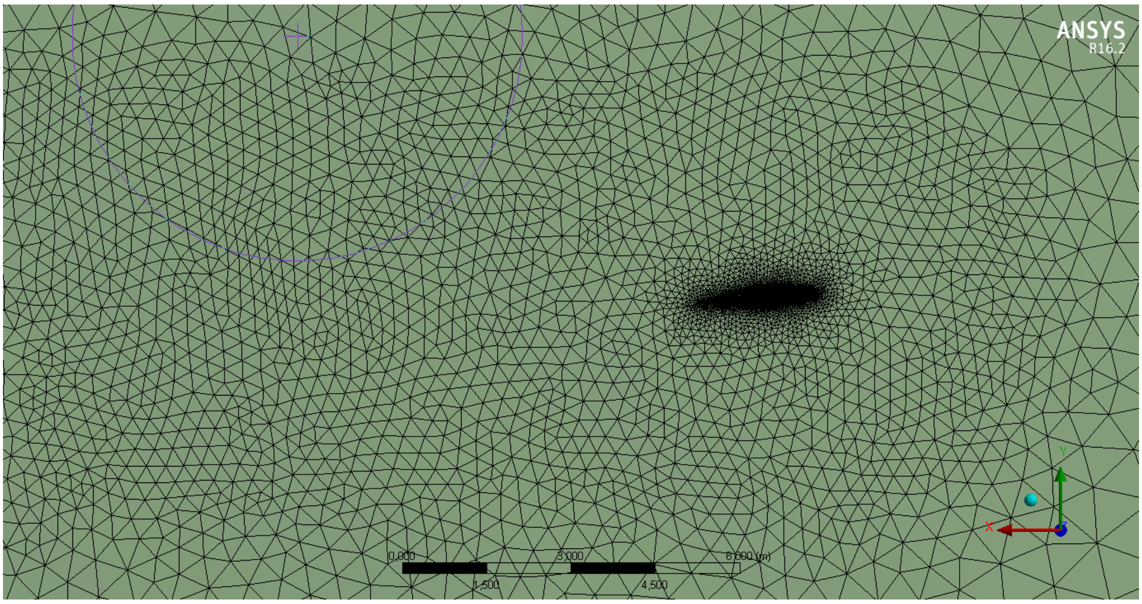
ANSYS
R16.2
0,000
3,000
6,000 (m)
1,500
4,500
y
x

Figure 4.12: Region of refinement of the final mesh

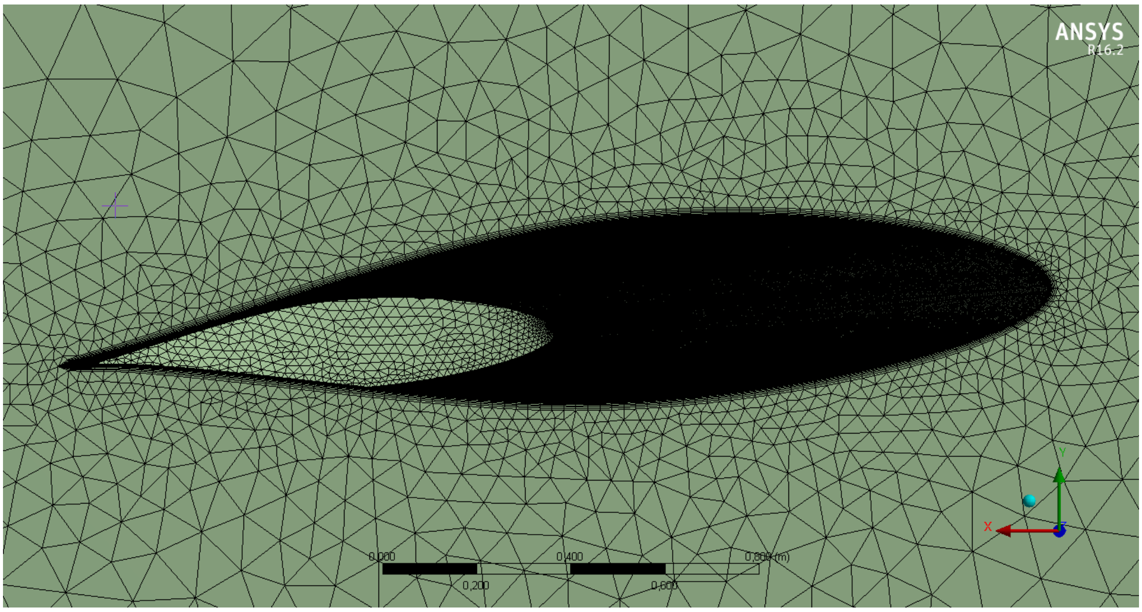
ANSYS
R16.2
0,000
0,400
0,800 (m)
0,200
0,600
y
x

Figure 4.13: Final mesh close to the airfoil

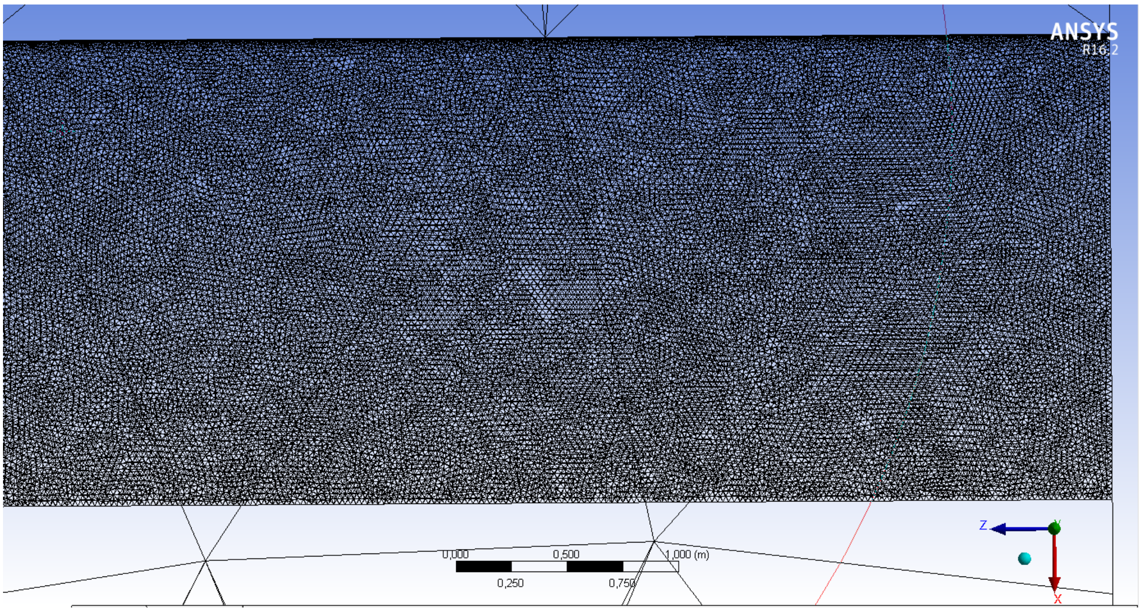

Figure 4.14: Detail of the mesh on the wing surface

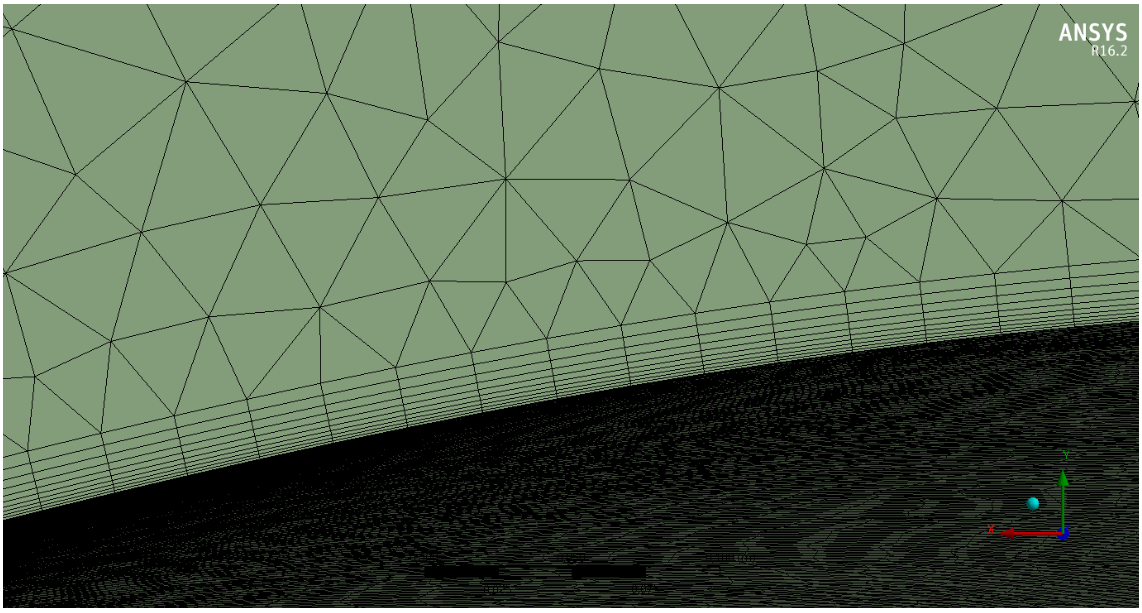

Figure 4.15: Detail of the inflation layer sorrounding the airfoil

4.3.3 Mesh statistics

It is important to know the quality of the mesh that has been created by ANSYS. If the quality of the mesh is not good enough, it can lead to wasted computation time or even to incorrect solutions. In order to state the characteristics of the mesh, ANSYS establishes a series of parameters that assert how good it is. The most relevant ones are:

- **Number of nodes and number of elements**. The elements of the mesh is each one of the subdomains in which it is divided. The nodes are the connections between these elements. These do not talk about the quality but are relevant in order to reduce the computation time.

The mesh for the cruise condition and 0 Cant Angle has been selected for giving information related to the statistics of the mesh. This is because all the other meshes have the same parameters than this one, and then the meshes have similar characteristics between them. This mesh has **1336777 nodes** and **4631616 elements**.

- **Aspect ratio of the elements**. The aspect ratio measures how stretch an element is. It is the relation between the highest side of an element and the smallest one. The ideal aspect ratio is 1, and its desirable values are below 100, although it is admitted to be higher in the inflation layers.

Aspect ratio	**Value**
Min.	1.1583
Max.	139.72
Average	7.2142
Standar deviation	9.7738

Table 4.3: Parameters for the Aspect Ratio of the mesh

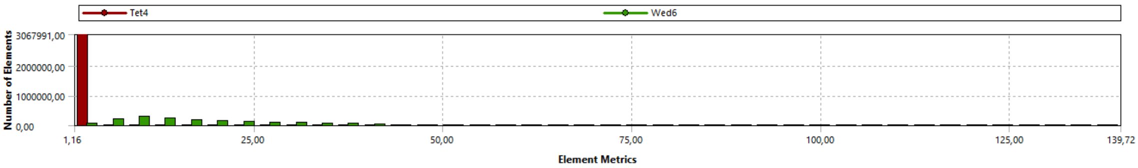

Figure 4.16: Mesh metrics of the Aspect Ratio

Figure 4.16 shows the number of elements of the mesh for each determined Aspect ratio. Then, by looking at this Figure and table 4.3 it can be seen how the majority of the elements have an aspect ratio very close to 1. There are some elements that have an aspect ratio above the maximum expected (100). However, these elements were allocated in the Inflation layer that is surrounding the wing, where the first layers use to have high aspect ratios.

- **Skewness**. The skewness determines how close to ideal (i.e., equilateral or equiangular) a face or cell is. Its ideal value is 0 and it should be below 0.98 in order to be acceptable.

Skewness	**Value**
Min.	1.382e-006
Max.	0.94804
Average	0.22671
Standar deviation	0.1281

Table 4.4: Parameters for the Skewness of the mesh

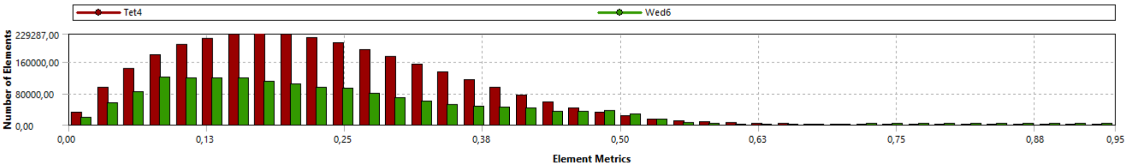

Figure 4.17: Mesh metrics of the Skewness

Taking a look at Figure 4.17, which shows the number of elements for each defined Skewness, and table 4.4 it can be seen how all the elements in the mesh are enclosed in the acceptable boundary in accordance with Figure 4.18. In this case, the average Skewness is 0.22. This, according also to Figure 4.18, is in the range of excellent elements based on Skewness.

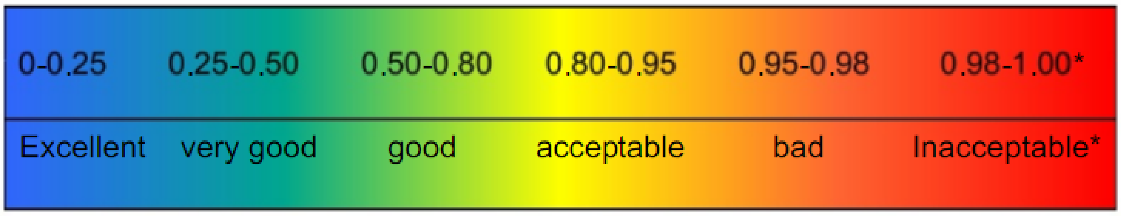

0-0.25	0.25-0.50	0.50-0.80	0.80-0.95	0.95-0.98	0.98-1.00*
Excellent	very good	good	acceptable	bad	Inacceptable*

Figure 4.18: Classification of the mesh quality metrics based on skewness

Chapter 5

Mathematical procedure

In this chapter, all the mathematical procedures followed to get to the final solution are going to be proposed. Prior to running all the cases in CFX, it is necessary to compute the Angle of Attack for cruise and gust. After calculating both parameters, all the calculations relating both flight conditions are presented. Finally, the study is divided into two branches with two different concepts: passive and active design.

5.1 Angles of Attack computation

5.1.1 Cruise

First of all, the Angle of Attack for cruise is computed. To calculate the Angle of Attack for the cruise state a Vortex Lattice Method has been used for the same wing under study[1]. The curve that has been obtained is the Lift coefficient (C_L) vs Angle of Attack (α) (see Figure 6.31). The Lift coefficient is the dimensionless parameter for measuring Lift and is given by:

$$C_L = \frac{L}{1/2\rho U_\infty^2 S} \tag{5.1}$$

In equation 5.1, ρ is the density, U_∞ is the velocity of the free-stream and S is the planform surface of the wing. For simplicity, when computing the Lift coefficient for wing+winglet, the used surface is the planform of the wing.

With this curve, and knowing the Lift coefficient for the aircraft at a certain cruise condition (In which Lift and weight are equal), the Angle of Attack is calculated by interpolation. See results in section 6.1.

5.1.2 Gust

Regarding the calculation of the gust Angle of Attack, the gust gradient at which it is found has to be settled. The selected gust gradient is H=12.5 MAC[2]. There are two main reasons for this choice. The first one is to consider the state of the art, since this is the maximum gust that has been considered historically by industry. Also, the second reason is because of computational difficulties. When the Angle of Attack is increased to high angles, the boundary layer separates, creating unstable vortices, which may lead to a transient solution, and then, the computation time increases and post-processing is much more time-consuming.

---

[1] The vortex Lattice Method (VLM) is a numerical method based on the thin-wing theory in which the aerodynamic forces are calculated using Horse-shoe votices.

[2] This gust gradient is within the regulations proposed by EASA: 30-350 ft

Once this gust gradient is decided, its topmost peak will be selected to compute the highest increase in loads that are produced by the gust, due to the fact that at this point the gust velocity is the highest, and so is the Angle of Attack, whose variation is defined as:

$$\Delta\alpha_{max} = atan(\frac{U_{ds}}{U_\infty}) \tag{5.2}$$

This variation will increase the Angle of Attack for gust with respect to the one at cruise, so the Lift and Drag will enlarge. All these computations have been calculated according to the regulations proposed in section 1.4.1. See section 6.2 for information relative to the calculation of the gust Angle of Attack.

5.2 Simulations for cruise in CFX

After calculating the Angle of Attack for cruise and the Angle of Attack for gust, 10 simulations are run in CFX for the cruise condition. Each simulation had the same conditions, and the only change is the Cant Angle. Varying this angle, different forces were obtained. The Forces that have been exported from the program are Lift and Drag in the wing and winglet separately. This separation is made because in this way, it will be possible to obtain the moment that the winglet is creating in its junction with the wing.

To see all these results for the cruise condition see sections 6.3.1 and 6.3.2.

5.3 Cant Angle for cruise

The Cant Angle for cruise is selected to be the Cant Angle for maximum aerodynamic efficiency. The aerodynamic efficiency is the relation between the Lift and Drag defined as (L/D). This Cant Angle will be fixed for the cruise conditon, so as to have a reference with which the gust loads are compared. The reason why the maximum aerodynamic efficiency point is selected is for optimizing the winglet for the cruise condition, so when a gust is not present, the performance of the aircraft is the best. It is computed as follows.

Since there are not infinite data points, the exact solution for the Cant Angle of maximum aerodynamic efficiency is discovered by doing some calculations. First of all, the point for maximum aerodynamic efficiency of the discrete data is selected. Afterwards, a second degree polynomial fit is performed with this data and the two adjacent points. The point at which the maximum L/D is found within this fit is finally selected for the position of the winglet at cruise. Once the position is calculated, this same procedure is made for all the other variables (Moment, Drag...) but in this case the unknown is the parameter and not the Cant Angle of the winglet.

For graphical information relating this computation see Figure 6.10.

5.3.1 Moment at the hinge

The moment that the air stream creates on the junction of the wing and the winglet is calculated with the isolation of the winglet Lift. Once this is isolated, the moment is expressed as the Lift times the distance from the center of pressure of the winglet[3] to the hinge (distance "d" in Figure 5.1). The equation that gives this distance is:

$$d = y_{cp} cos(\theta_w) \tag{5.3}$$

In equation 5.3, y_{cp} is the position of the center of pressure of the winglet w.r.t. the hinge, which in this case, will be considered to be at the y-position of the MAC.

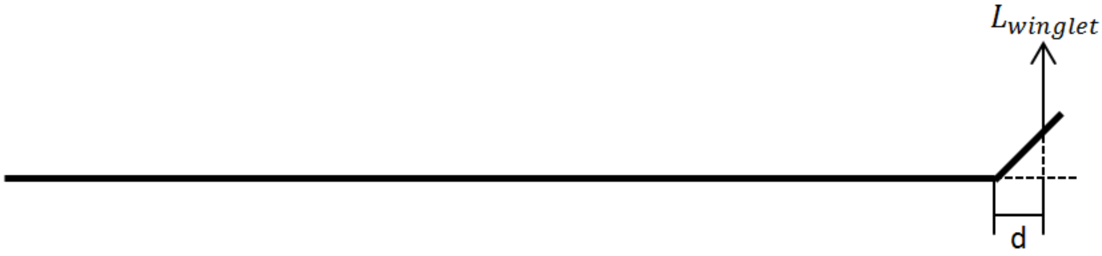

Figure 5.1: Schematic of the Lift force in the winglet and the point of application

Then, the equation for the moment at the hinge is:

$$M(\theta_w) = y_{cp} \cdot cos(\theta_w) \cdot L_{winglet} \tag{5.4}$$

To see the results for the moment at cruise see Figure 6.11.

5.4 Simulations for gust in CFX

Afterwards, the same number of simulations are run but for the condition of gust, varying also the Cant Angle. The gust state has been considered as a variation in the Angle of Attack with respect to the Angle of Attack at cruise. In regard to the calculation of the gust loads, there are two conceptual approaches as stated before: Passive and Active. To see all the results relative to the simulations for gust see section 6.3.3.

5.5 Passive design mathematical model

5.5.1 Model proposition

For the passive design a torsion spring is allocated in the hinge between the wing and the winglet. To simulate so, a simplified structural model in which the only variable is the stiffness of this spring is created. In this model, the moment at the junction varies as a function of the spring rigidity. The variation of the moment with respect to the Cant Angle is selected to change linearly according to:

$$M = K \cdot (\theta_w - \theta_0) \tag{5.5}$$

---

[3] The center of pressure is the point where the surface force of the aircraft wing is concentrated

In equation 5.5, θ_0 is the natural position of the winglet and K is the torsion spring rigidity. The natural position of the winglet is the Cant Angle when the aircraft is stop. This is found because when $\theta_w = \theta_0$ there is no moment at the hinge and then the winglet does not move.

Now, the objective is to have an idea of how the performance of the aircraft changes with the flexibility of the winglet. For that, a range of K's is selected. This range goes from 2 to 200 N.m/^{o}.

5.5.2 θ_0 calculation

With the stated range of rigidities, it is firstly calculated the natural position of the winglet for each K (θ_0). θ_0 is computed by introducing into equation 5.5 the Cant Angle and moment at cruise:

$$\theta_0(K) = \theta_{w,cruise} - M_{cruise}/K \tag{5.6}$$

In equation 5.6, $\theta_{w,cruise}$ is the Cant Angle for cruise and M_{cruise} is the moment for cruise. With the calculation of θ_0 and he previous calculation of the cruise Cant Angle, the variation of the spring with moment for each stiffness is totally defined.

The results for θ_0 can be seen in Figure 6.20.

5.5.3 Equilibrium Cant Angle

If we imagine a flexible winglet that can move according to the air stream, in the presence of a gust it would experience an increase in Lift and consequently in moment. This enlargement in Lift and moment would make the winglet to rotate upwards passively. If a spring is located at the winglet hinge, at some Cant Angle the moment created by the gust and the moment produced by the spring have to be in equilibrium. This final position depends on the gust aggressiveness and on the spring rigidity. For example, if the spring was very stiff, the equilibrium moment would be found at a lower Cant Angle than if it was not. This is because the moment created by the spring increases with Cant Angle according to 5.5, and then a lower angle would be needed for compensating the moment created by the gust.

Then, the final position of the winglet for gust is calculated by computing the intersection between the structural model in equation 5.5 and the curve of moment vs θ_w obtained with the CFD simulation. This intersection is the equilibrium point and is different for each K.

Since the CFD data is discrete, the intersection for each K is calculated with interpolation between the points of the graph. In order to interpolate such data, the curve of moment is approximated to a 3 degree polynomial, since it is seen to have an almost perfect polynomial shape. Once the equilibrium Cant Angle of the winglet is computed for each spring, another interpolation is made in order to obtain the Lift and Drag for each K.

In order to have a visual approach of how this equilibrium Cant Angle is computed, see Figure 6.21

5.5.4 Load Factor (n)

As soon as equilibrium position and forces have been computed for each spring, it is calculated the final load factor for gust. The load factor is a relevant figure for aviation. It represents the ratio between the Lift of an aircraft and its weight. So if, for instance, the load factor was 2, it would mean that the load that it is experiencing is twice its weight. The load factor is desired to be as close to one as possible for the cruise condition since the Lift generated in cruise has to be equal to the weight for maintaining level flight. In this case, the generated Lift is the Lift for gust and the weight is the calculated Lift for cruise:

$$n = \frac{L_{gust}}{L_{cruise}} \tag{5.7}$$

In equation 5.7, L_{gust} is the Lift for gust and L_{cruise} is the Lift for cruise. The final load factor computed for each spring rigidity will be compared with the condition in which the winglet is maintained at the cruise Cant Angle ($K = \infty$).

All these calculations are explained throught a flowchart in Figure 5.5.4.

Once the final load factor has been defined, some other calculations are going to be made so as to assess the differences between each spring type. First of all, the maximum value that K can adopt is going to be calculated. This K value is set for the K at which the load factor begins to be higher than that one for cruise. See section 6.4, Figure 6.22.

Furthermore, the percentage of load factor alleviation for a gust is going to be calculated as a function of K. This figure shows how much the load factor is alleviated in general terms, and is defined as:

$$\%n_{allev.}(K) = \frac{n_{gust,\theta=\theta_{cruise}} - n_{gust}(K)}{n_{gust,\theta=\theta_{cruise}}} \tag{5.8}$$

In equation 5.8, $n_{gust,\theta=\theta_{cruise}}$ is the load factor for gust when the Cant Angle is at the cruise position and $n_{gust}(K)$ are the different load factors founded for each different K. The reason why it is compared with the condition at which $\theta = \theta_{cruise}$ is because this is the reference condition for a rigid winglet. See section 6.4 Figure 6.24.

Besides, the percentage of abatement of the variation in load factor from the cruise condition to the gust state is computed. This variable is also relevant, since it expresses the assuagement of the total load increase created by the gust, taking as a reference the load factor 1 for cruise instead of a load factor of 0. As an explicative approach: if, for instance, the load factor was 2, this would mean that the load increase is a 100%; the proposed variable would tell us about the load alleviation over this 100%, and not about the total 200% with respect to the 0 reference. It is defined as:

$$\begin{aligned}\%\Delta n_{allev.}(K) &= \frac{(n_{gust,\theta=\theta_{cruise}} - n_{cruise,\theta=\theta_{cruise}}) - (n_{gust}(K) - n_{cruise,\theta=\theta_{cruise}})}{n_{gust,\theta=\theta_{cruise}} - n_{cruise,\theta=\theta_{cruise}}} \\ &= \frac{(n_{gust,\theta=\theta_{cruise}} - 1) - (n_{gust}(K) - 1)}{n_{gust,\theta=\theta_{cruise}} - 1}\end{aligned} \tag{5.9}$$

In order to have information relating this parameter, see section 6.4 Figure 6.25.

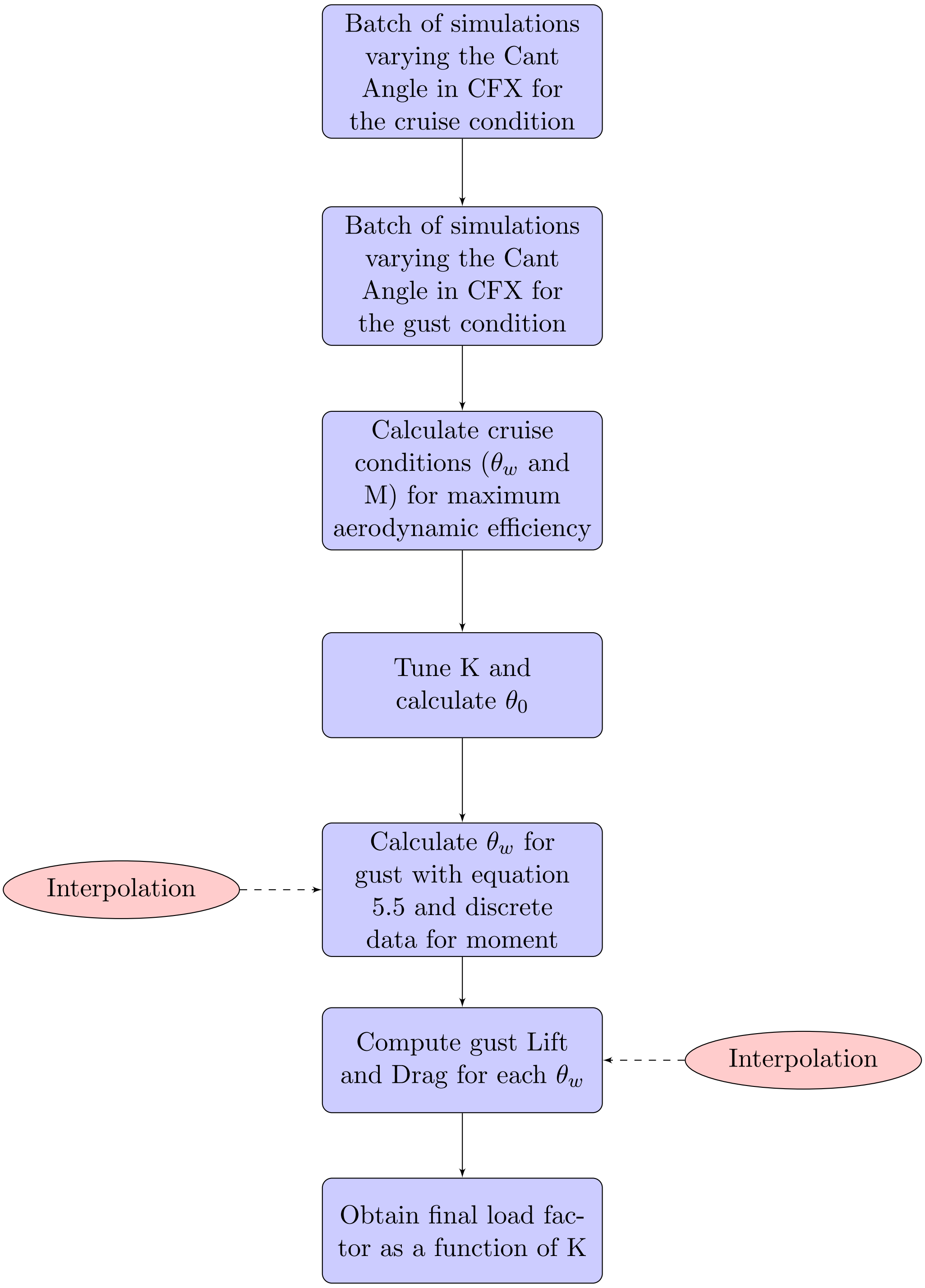
Batch of simulations varying the Cant Angle in CFX for the cruise condition
Batch of simulations varying the Cant Angle in CFX for the gust condition
Calculate cruise conditions (θ_w and M) for maximum aerodynamic efficiency
Tune K and calculate θ_0
Interpolation
Calculate θ_w for gust with equation 5.5 and discrete data for moment
Compute gust Lift and Drag for each θ_w
Interpolation
Obtain final load factor as a function of K

Figure 5.2: Flowchart for the mathematical computation of the passive case.

5.5.5 Evolution with Angle of Attack and time

After computing all the parameters for a gust scenario, some more simulations are performed in the same way for Angles of Attack in between the one for cruise and the one for gust. In all these simulations, the equilibrium Cant Angle of the winglet is obtained by calculating the intersection between equation 5.5 and the variation of moment calculated numerically for each Angle of Attack as was done for the gust AoA. All the results for these intermediate Angles of Attack are on Appendix A.

In this case, instead of selecting a range of K's, an exact value for K is selected so that it is possible to have an idea of the performance with the Angle of Attack.

After calculating the final winglet position for each intermediate Angle of Attack, every parameter like Lift or Drag is calculated with an interpolation similar to that one used for the case of gust, using the equilibrium Cant Angle. With all these points, the evolution of Lift coefficient (Figure 6.27), load factor (Figure 6.28) and Drag coefficient (Figure 6.29) is computed as a function of the Angle of Attack. The Drag coefficient is given in a similar way as the Lift coefficient:

$$C_D = \frac{D}{1/2\rho U_\infty^2 S} \tag{5.10}$$

Load factor is finally computed as a function of time (Figure 6.26) as follows. For all the Angles of Attack, it is going to be assumed the velocity of the gust for each point as a function of the variation of the Angle of Attack from cruise is:

$$U = \tan(\Delta\alpha)\, U_\infty \tag{5.11}$$

In equation 5.11, U is the velocity of the gust at each point provided by equation. With this, the evolution of the load factor as a function of time is going to be calculated with equation 1.1. If the space travelled by the airplane is isolated it is obtained that:

$$s = \cos^{-1}\left(1 - \frac{\tan(\Delta\alpha)\, U_\infty 2}{U_{ds}}\right)\frac{H}{\pi} \tag{5.12}$$

With this travelled distance in the gust, the time is obtained as:

$$t = \frac{s}{U_\infty} \tag{5.13}$$

5.6 Active design mathematical model

The active case is the one in which the final position of the spring can be manipulated by means of an actuator. In this case, the final position of the winglet is selected so as to provide the lowest load factor for gust. In this case, the moment will be assumed to also change linearly with the Cant Angle with the following expression:

$$M(\theta_w) = c_1 \cdot \theta_w + c_2 \tag{5.14}$$

This variation is chosen in order to have a rule of how the actuation varies, and then it is possible to have a model for evaluating the conditions for the angles of attack in between cruise and gust. However, a better model for this variation should be calculated in further developments in order to optimize the design even more.

In this case, the two constants are not calculated as in the active design. Now they are computed with a system of two equations with two unknowns, in which the inputs are the moment and angle for both, the cruise and gust conditions, and the variables of the system are both, c_1 and c_2.

Once these constants are obtained, A similar approach as for the passive case is performed for each Angle of Attack by computing the intersection between equation 5.14 and the discrete data for the moment in the winglet.

For information regarding the active design see section 6.5

Chapter 6

Results

6.1 Cruise Angle of Attack

The cruise condition is that one in which the weight of the aircraft is balanced by the Lift force, being both in equilibrium. In this way, there will not be acceleration in the vertical direction and the aircraft will hold its altitude.

The weight for cruise used in the VLM is 5900 kg, the altitude is 4755 m ($\rho = 0.75567 \quad kg/m^3$, $T = 257.25 \quad K$, $P = 55800 \quad Pa$)[1] and the aircraft airspeed is 87.5 m/s. With al this, the Lift coefficient will be:

$$C_L = \frac{W}{1/2 \cdot \rho \cdot U_\infty^2 \cdot S} = 0.54798 \tag{6.1}$$

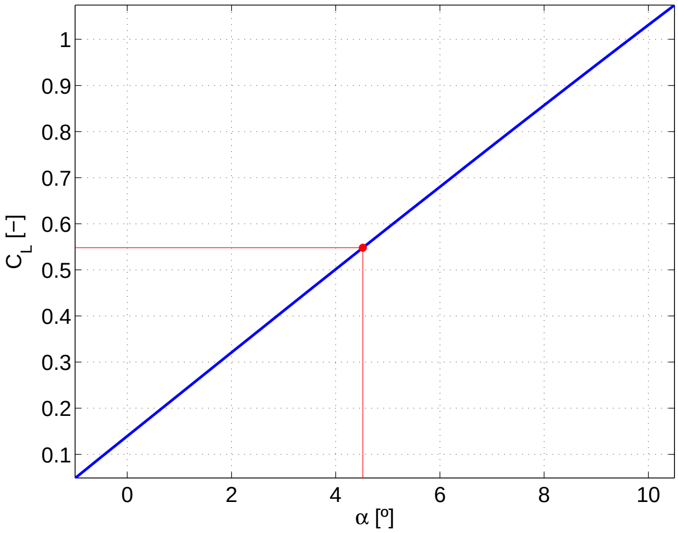

Figure 6.1: Lift coefficient vs Angle of Attack for the VLM results

With this Lift coefficient, the Angle of Attack is found with the VLM results in Figure 6.1 by interpolation. **It is found at 4.5º**. This is the angle that is going to be used for the cruising condition in ANSYS CFX. It is important to notice that between the VLM and CFD results there will be some differences and then the Results of the Lift will not be exactly the same. However, this first approach for the Angle of Attack will be very close to the Angle of Attack at cruise for this weight.

---

[1] These characteristics of the fluid are based on the ISA model

6.2 Gust Angle of Attack

In order to compute the Angle of Attack for the gust under consideration, the following data is used:

Aircraft characteristics	
Altitude	4755 m
ρ	0.75567 Kg/m^3
MTOW	8100 Kg
MZFW	4580 Kg
MLW	7290 Kg
Z_{mo}	15000 m

Table 6.1: Characteristics of the aircraft for the gust calculations and the flight conditions

With these aircraft characteristics, the weight selected for the VLM calculations in section 6.1 will be the weight for a condition at the middle of cruise, since its weight is between MTOW and MZFW.

The reference velocity is 13.316 m/s in EAS, following the guidance stated before by paragraph CS 25.341, which in TAS will be:

$$TAS = \frac{EAS}{\sqrt{\sigma}} = 16.954 m/s \tag{6.2}$$

where σ is the relation in between the actual density and the density at sea level (1.225 Kg/m^3).

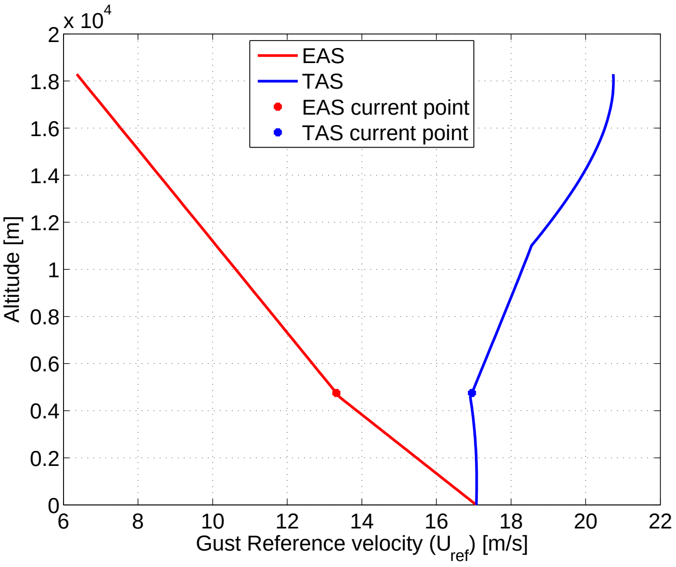

Figure 6.2: Evolution of the reference velocities with altitude

This all can be seen in Figure 6.2, in which the evolution of TAS and EAS of the reference velocity are plotted. In this plot, the current point under calculation is highlighted.

The selected H for the gust is 12.5 times the Mean Aerodynamic chord as stated before, which is 73.782 ft (22.489 m). This will not provide the maximum possible change in Angle of Attack, which would be given by a gust with H=350 ft, but it can provide a sense on how the aircraft behaves under the presence of gusts.

Now, with all the provided data, putting all into the previously stated equations for the calculation of the gust velocity, the following results are obtained:

$$R_1 = 0.9 \tag{6.3}$$

$$R_2 = 0.56543 \tag{6.4}$$

$$F_{gm} = 0.69493 \tag{6.5}$$

$$F_{gz} = 0.80315 \tag{6.6}$$

$$F_{g0} = 0.74904 \tag{6.7}$$

$$F_g = 0.82859 \tag{6.8}$$

$$U_{ds} = 10.838 \tag{6.9}$$

$$\Delta\alpha = atan\left(\frac{U_{ds}}{U_{inf}}\right) = atan\left(\frac{10.838}{87.5}\right) = 7^\circ \tag{6.10}$$

Then, by adding the cruise Angle of Attack and the gust Angle of Attack, **the final Angle of Attack for gust is 11.5°**.

6.3 CFX results

6.3.1 Contours of pressure for cruise condition

Here, in Figure 6.3 it is possible to see the contours of pressure for cruise condition at Cant Angles of 0, 5, 10 and 20 degrees. This angles are selected as a sample of the whole set of computed angles. It can be seen how the pressure distribution in the wing and the winglet varies as the Cant Angle varies. This different pressure distribution, will make the total integrated force over each surface to be different, and then distinct forces will be found as function of the Cant Angle.

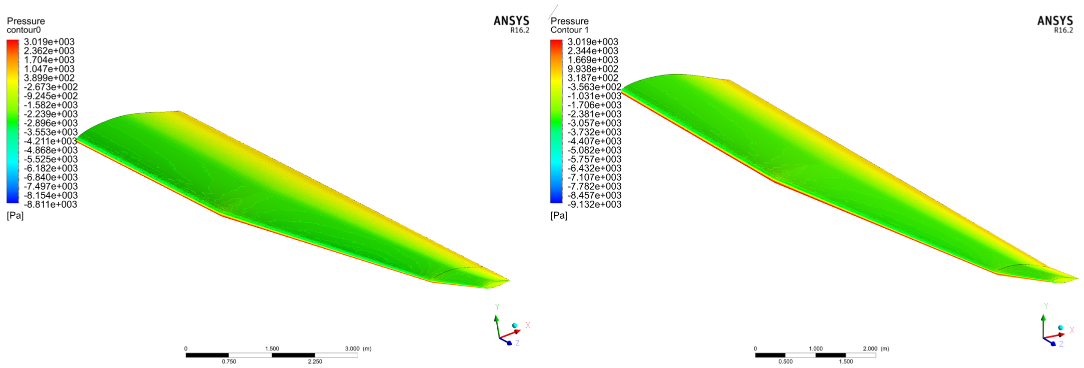

(a) Contours of pressure for cruise condition at a Cant Angle of 0° (b) Contours of pressure for cruise condition at a Cant Angle of 5°

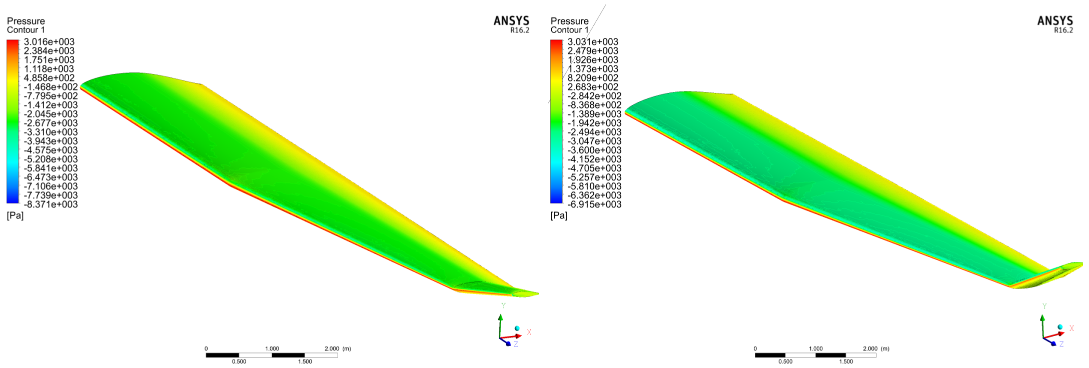

(c) Contours of pressure for cruise condition at a Cant Angle of 10° (d) Contours of pressure for cruise condition at a Cant Angle of 20°

Figure 6.3: Contours of pressure for Cant Angle of 0, 5, 10 ad 20 degrees for Cruise condition.

6.3.2 Cruise results

Once all the forces have been integrated over each surface, it is possible to divide all of them in the ones produced on the winglet and those on the wing.

The following Figures show the different forces calculated in the wing and winglet as functions of the Cant Angle. In order to be able to calculate the moment produced on the winglet, the Lift and Drag forces have been computed separately on both surfaces. Figure 6.4 shows the Lift produced by the wing isolated when the Cant Angle varies. Figure 6.5 shows the evolution of Drag on the wing. Figure 6.6 provides information about the winglet

Lift and 6.7 plots the Drag on it. The next ones (6.9 and 6.8) sum up both contributions from the wing and winglet. Finally, Figure 6.10 plots the results for the Aerodynamic efficiency. It is important to notice that the range of angles selected is in between 0 and 80 degrees, since for angles higher than this, the generated mesh does not behave well and the results are incorrect. The whole set of calculated angles is: 0,5,10,20,30,40,50,60,70 and 80.

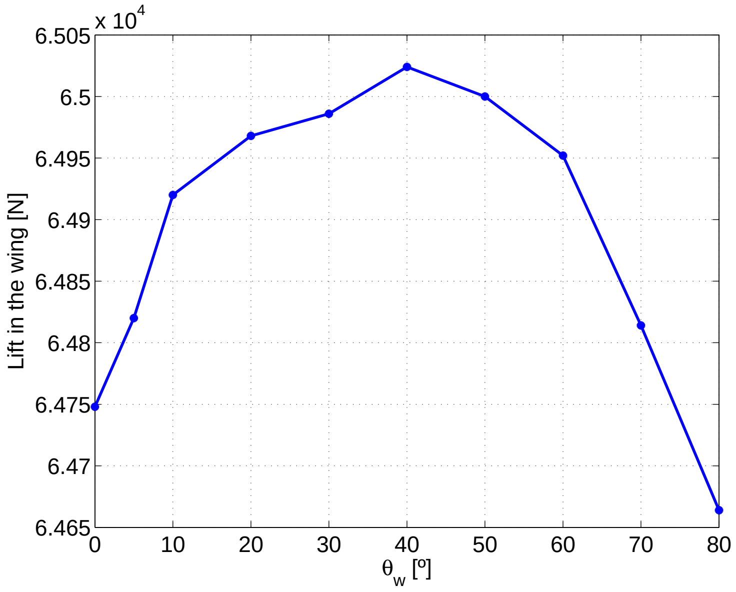

Figure 6.4: Variation of the Lift in the wing as a function of the Cant Angle

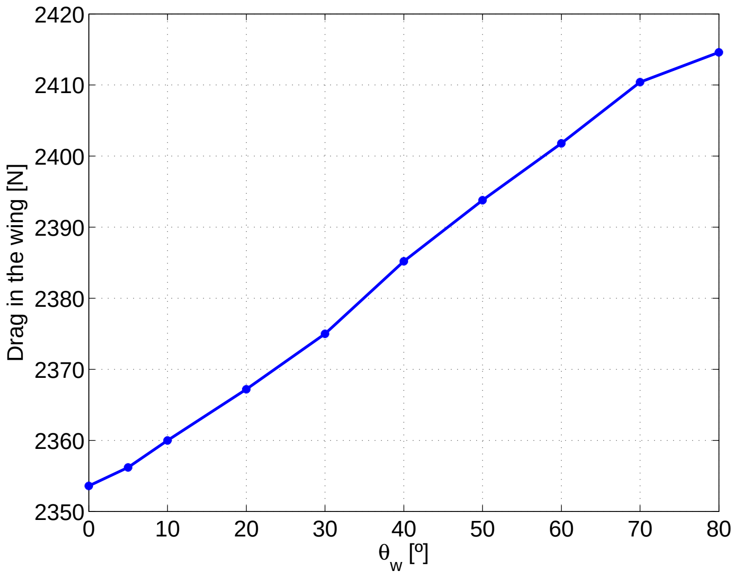

Figure 6.5: Variation of the Drag in the wing as a function of the Cant Angle

When looking at the Lift in the wing, it can be appreciated that it grows systematically until a Cant Angle of 40° at which it begins to decrease.

The Drag in the wing behaves in a different way since it grows as the Cant Angle does, and does not decrease at any moment.

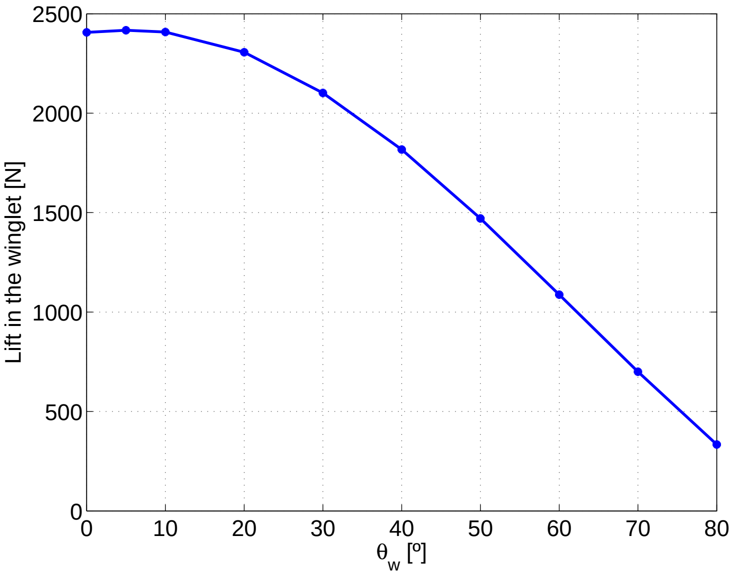

Figure 6.6: Variation of the Lift in the winglet as a function of the Cant Angle

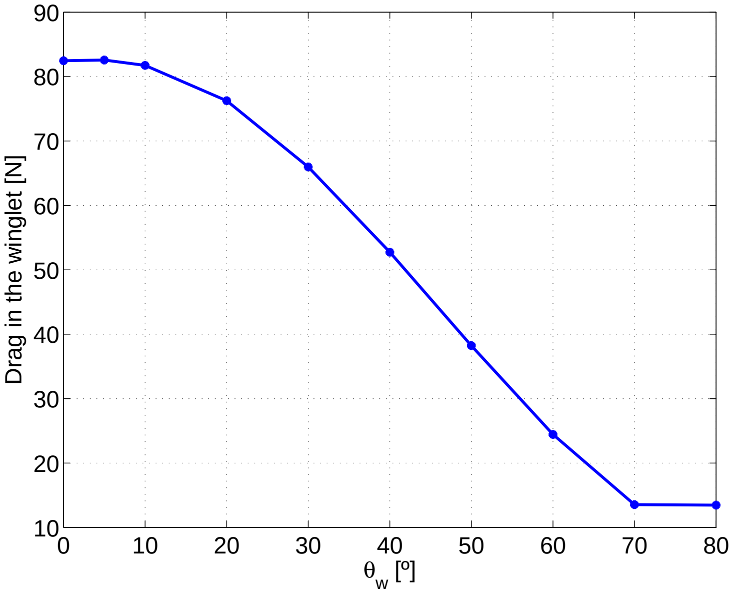

Figure 6.7: Variation of the Drag in the winglet as a function of the Cant Angle

The Lift and Drag in the winglet have been plotted as the total Lift that is generated. This means that it is not the Lift generated by one isolated winglet but by the two winglets of the aircraft at the same time. It is appreciated that the Lift in this part grows from 0 to 5 degrees, and later on it begins to decrease regularly until the last considered angle. Regarding the Drag, it can be seen that it behaves in a similar way but the difference is that it stabilizes at an angle of 75º. The reason why in the figure a stabilization is seen is because a minimum fo the Drag should be found at around 75°, but since the data is discrete, there is no information regarding this point.

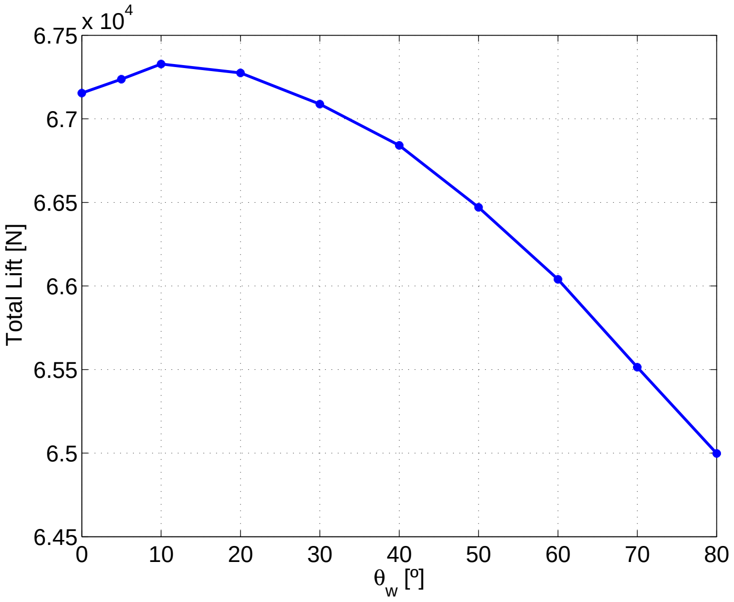

Figure 6.8: Total Lift as a function of the Cant Angle

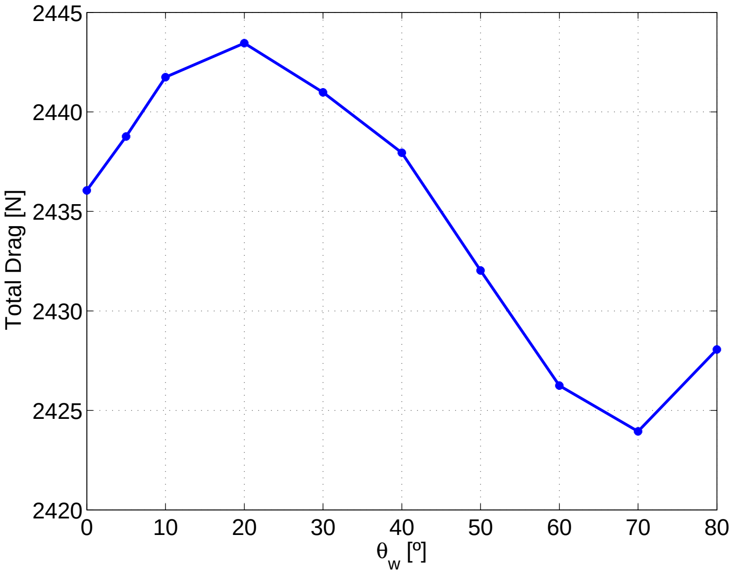

Figure 6.9: Total Drag as a function of the Cant Angle

The graphs for the Total Lift and Total Drag sum up the contribution of wing and winglet. Concerning Lift, the shape of the curve resembles the shape of the graph that showed the Lift on the winglet, growing at the beginning and decreasing later. The Drag has a similar shape as the Lift until the Cant Angle is at 70°, where it begins to grow again.

Now that all the results have been presented, Figure 6.10 shows the aerodynamic efficiency of the aircraft as a function of the winglet angle.

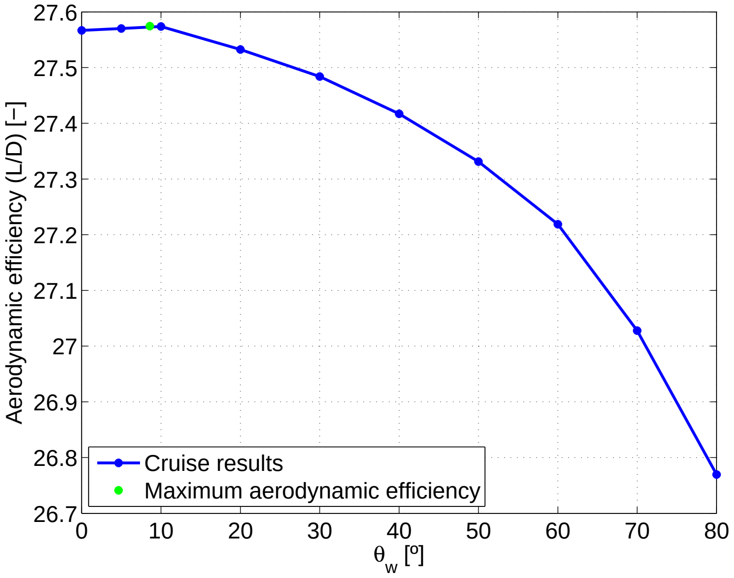

Figure 6.10: Aerodynamic efficiency as a function of the Cant Angle

The green point in Figure 6.10 is the point of Maximum aerodynamic efficiency, that has been calculated by following the guidelines of Chapter 5 . **This angle is 8.6º** and the Aerodynamic efficiency is **L/D=27.574**. Then, the winglet Cant Angle for cruise is selected to be in this position for all the computed cases. In this way, the winglet is optimized for the cruise condition.

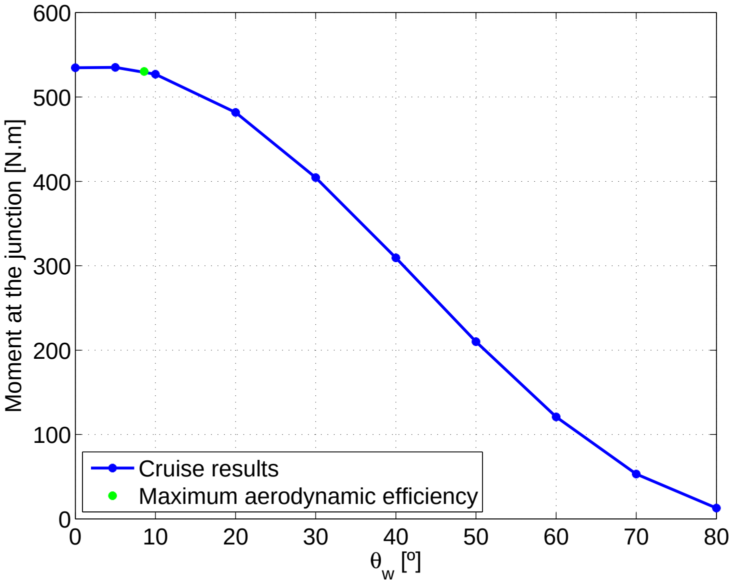

Figure 6.11: Moment at the hinge as a function of the Cant Angle

Figure 6.11 shows the Moment at the hinge calculated following 5.4. It is important to notice that the moment that is plotted is that one produced by one winglet, and not by both, as happened with the Lift graph. Finally, table 6.2 summarizes the results of all the variables for the maximum aerodynamic efficiency.

Maximum Aerodynamic Efficiency	
L_{wing} [N]	64897
D_{wing} [N]	2358.9
$L_{winglet}$ [N]	2413.3
$D_{winglet}$ [N]	82.105
$(L/D)_{max}$ [-]	27.574
$M_{(L/D)_{max}}$ [N.m]	524.96

Table 6.2: Summary of results for Maximum Aerodynamic efficency

6.3.3 Gust results

Now that all the discrete data has been presented for the cruise condition, the state of gust has to be analyzed. Figures 6.12 and 6.14 show the Lift in the wing and winglet respectively for a gust of with an Angle of Attack of 11.5 degrees. The Drag in the wing and winglet is provided by Figures 6.13 and 6.15 respectively. The total Lift and Drag for this gust are plotted in Figures 6.16 and 6.17. It can be seen how almost all these graphs show a very similar pattern to the one of cruise. However, there are some remarkable facts in Figure 6.17. In this picture, it can be appreciated how the total Drag for this condition follows a very strange pattern. It goes to a minimum, and comes back again to a maximum after this valley that appears in 60 degrees.

Figure 6.18 shows the Moment created by the air stream at the junction between the wing and the winglet for gust. This moment will have to be in equilibrium with the one created by each spring.

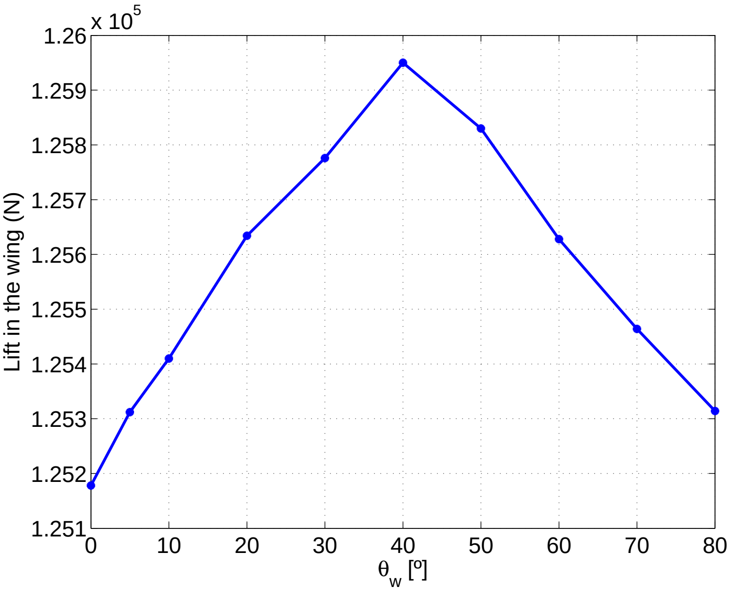

Figure 6.12: Variation of the Lift in the wing for a gust with AoA 11.5° as a function of the Cant Angle

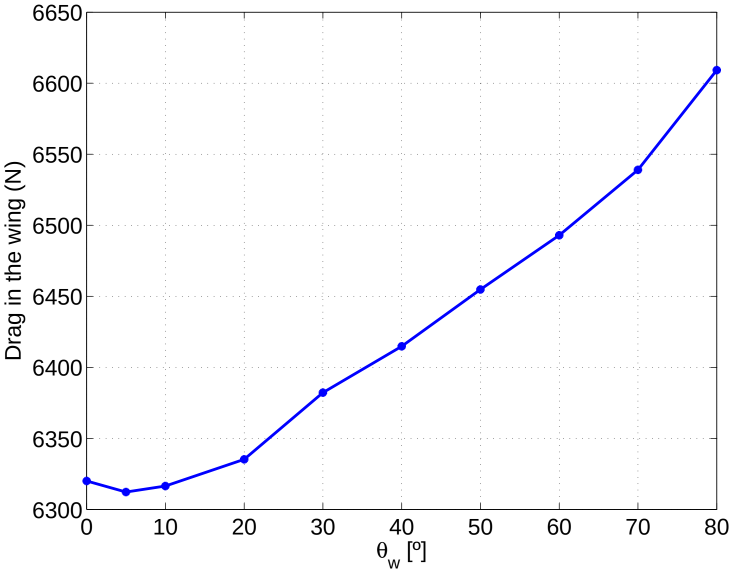

Figure 6.13: Variation of the Drag in the wing for a gust with AoA 11.5º as a function of the Cant Angle

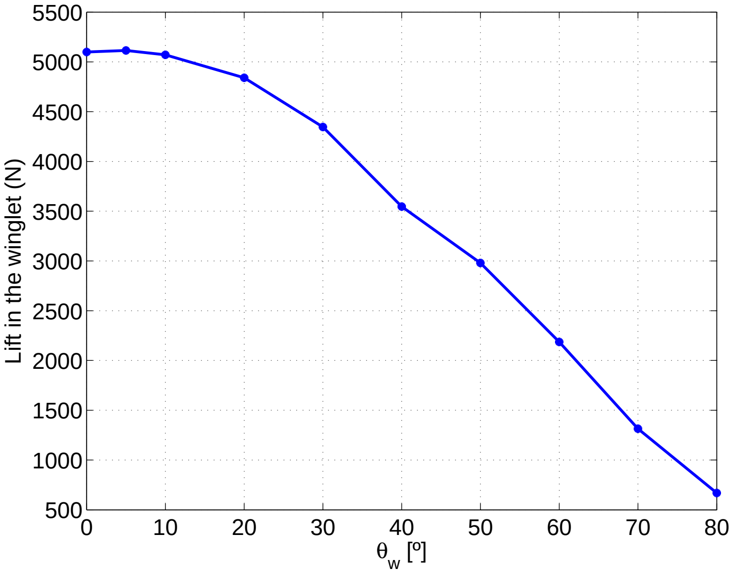

Figure 6.14: Variation of the Lift in the winglet for a gust with AoA 11.5º as a function of the Cant Angle

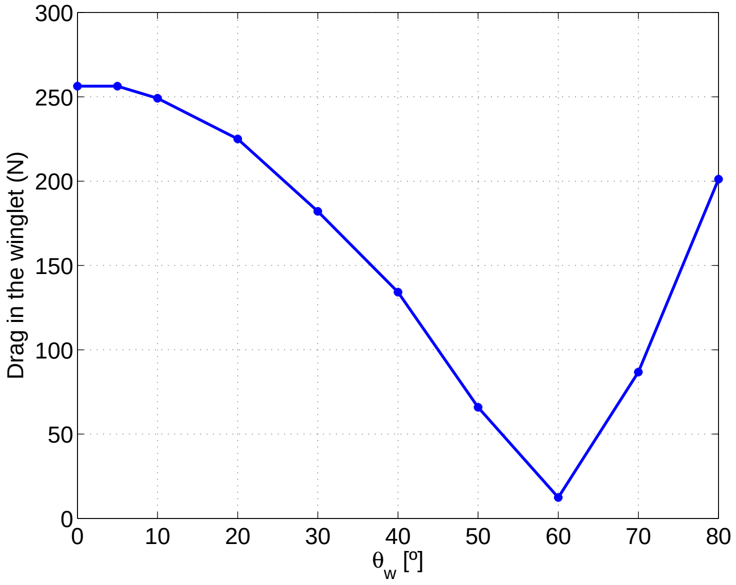

Figure 6.15: Variation of the Drag in the winglet as a function of the Cant Angle

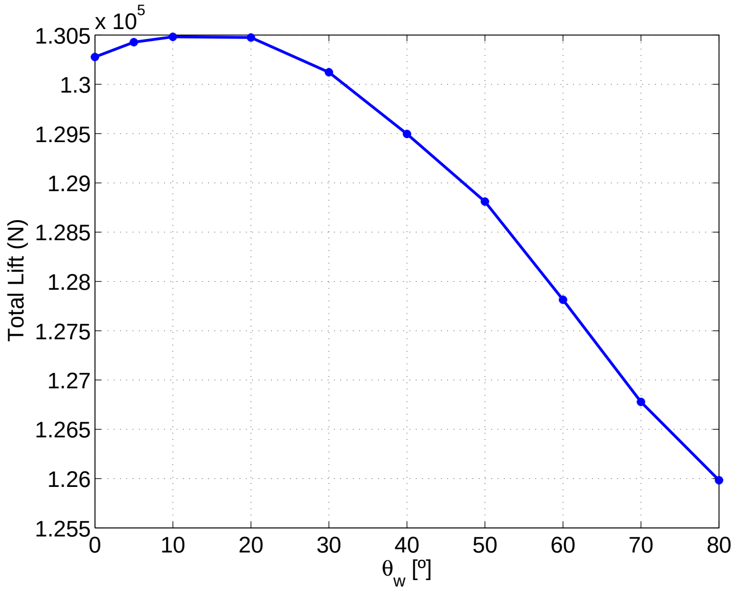

Figure 6.16: Total Lift for a gust with AoA 11.5° as a function of the Cant Angle

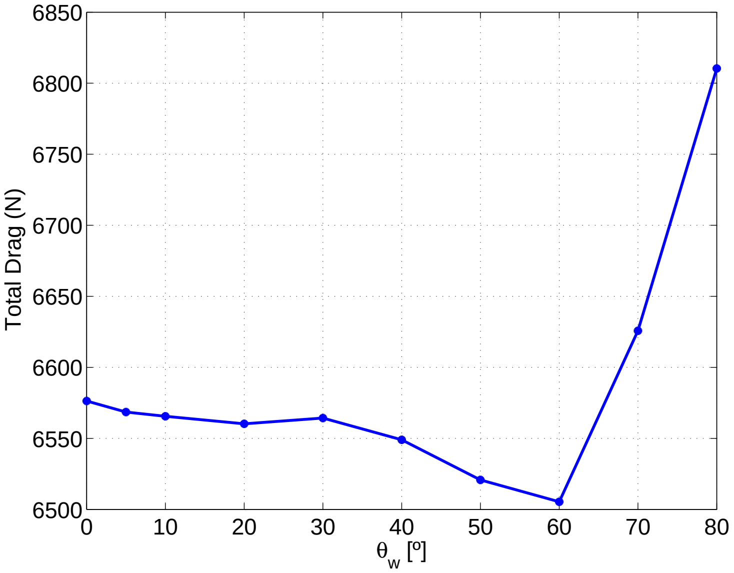

Figure 6.17: Total Drag for a gust with AoA 11.5° as a function of the Cant Angle

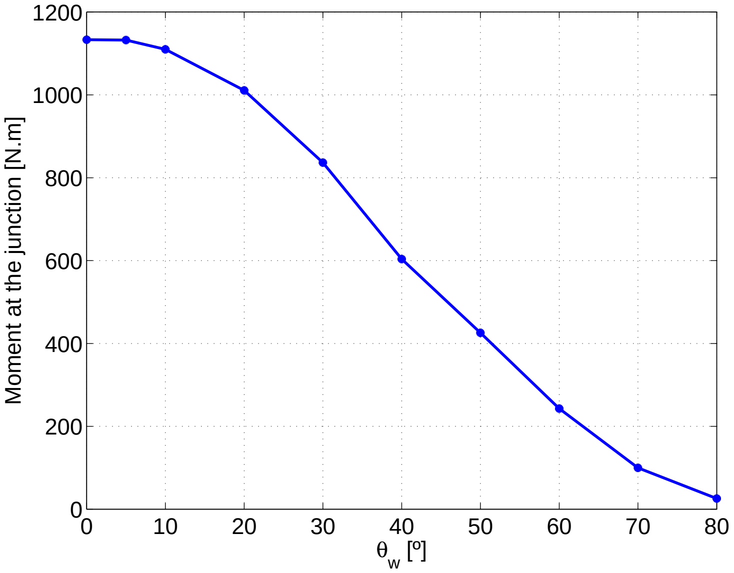

Figure 6.18: Moment for a gust with AoA 11.5° as a function of the Cant Angle

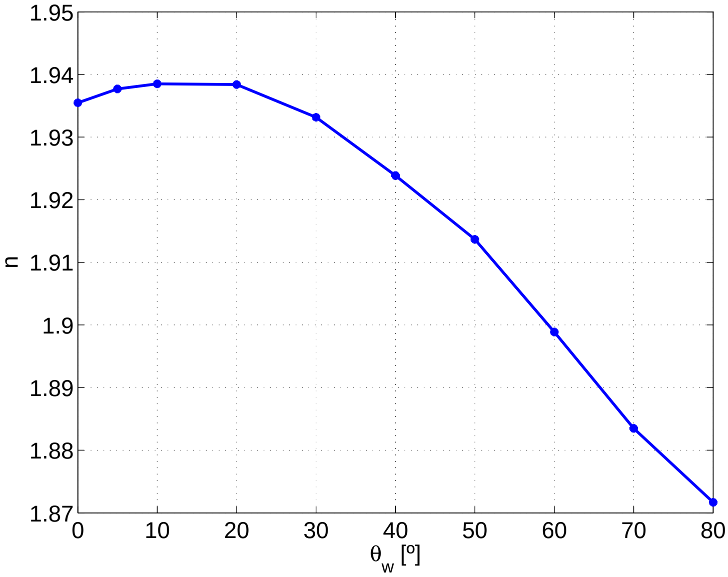

Figure 6.19: Load factor for a gust with AoA 11.5º as a function of the Cant Angle

In Figure 6.19 it can be seen the load factor for the gust condition. The reference under consideration is the Lift of the aircraft at cruise conditions ($\theta_w = 8.6^o$).

6.4 Passive design analysis

As mentioned above, this case will comprise the design in which a torsion spring is between the wing and the winglet and its movement is passive depending on the flight conditions. The only variable for the proposed structural model is the torsion stiffness of the spring. Now, the results for each considered spring are going to be proposed. The selected range of K's go from 2 to 200 N.m/º.

Firs of all, Figure 6.20 shows the natural position of the winglet as a function of the spring rigidity. It can be seen that for low values of K, the θ_0 also goes to very negative values, which may be an impediment as will be explained later.

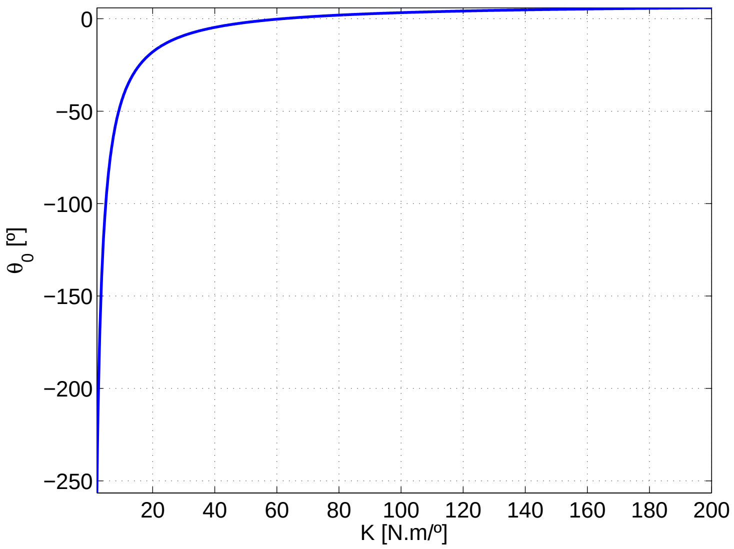

Figure 6.20: Natural position(θ_0) of the winglet as a function of the spring rigidity for a cruise Cant Angle of 8.6º

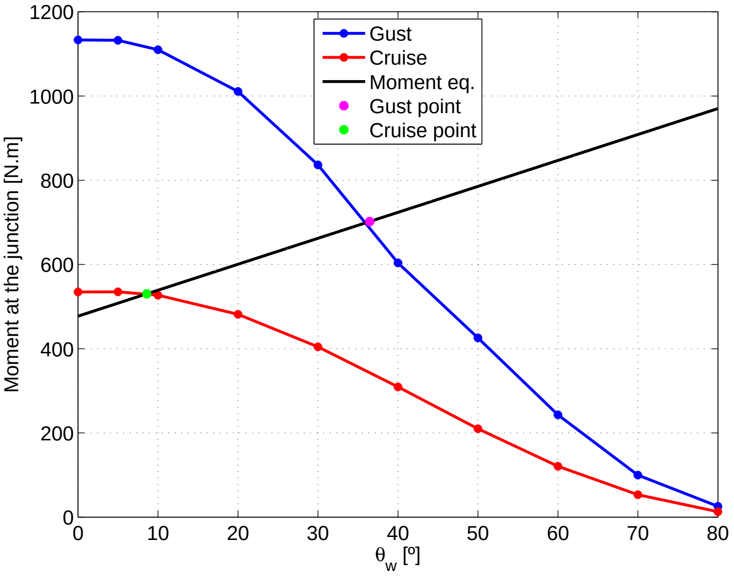

Figure 6.21: Equilibrium of moments for cruise and gust for the minimum value of K

Figure 6.21 is a sketch of how the final position of the winglet is calculated for each rigidity. With K, and the previously calculated θ_0, the variation of the moment in the winglet changes linearly with the Cant Angle, passing through the selected point at cruise. The final Cant Angle is computed in the intersection of this line with the interpolation of the discrete data.

The maximum value that K can adopt is calculated by means of Figure 6.22. In this graph, the final load factor as a function of the spring rigidity is plotted. It can be seen how the load factor grows systematically as the spring rigidity does. However, if the value of the load factor is higher than that for the cruise Cant Angle, the effect of having a flexible winglet would not make sense. This is the point that limits the maximum value for

K, which is marked with a black line, and has a value of 163.58 N.m/° (9372.4 N.m/rad). The load factor at this point is $n_{\theta_w=8.6} = 1.9384$, and is marked with a green point.

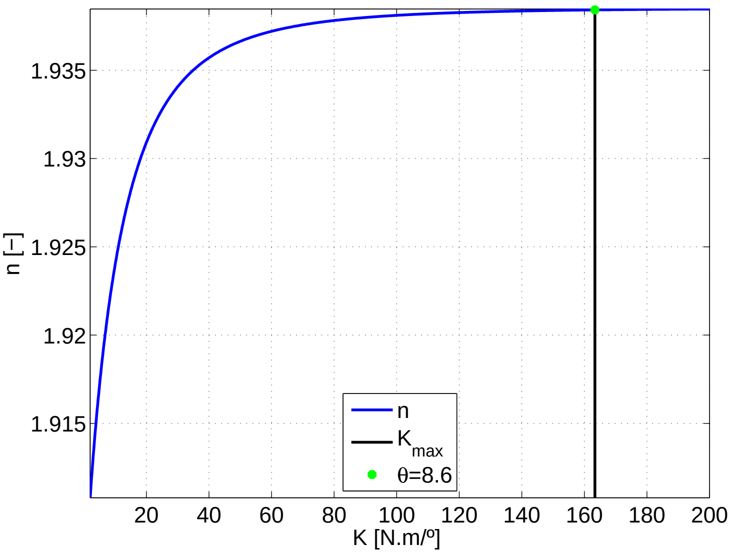

Figure 6.22: Final Load factor for a gust with AoA 11.5° as a function of the spring rigidity

Besides, Figure 6.23 shows the final equilibrium Cant Angle of θ_w for this gust, calculated as detailed in Figure 6.21. This final value of θ_w will have an asymptote in $\theta_w = 8.6$ when K is infinite, which is obvious, since this K would mean that the winglet is rigid and then the Cant Angle would not change. In this plot, the range of K has been extended to see this effect.

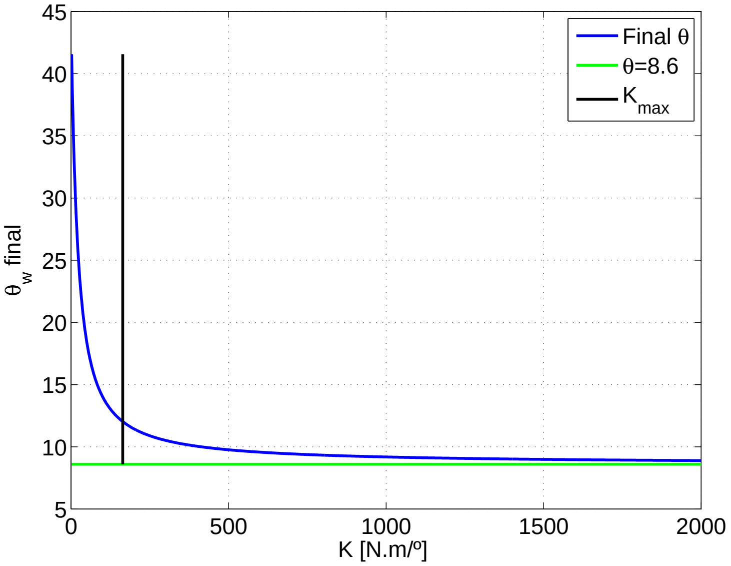

Figure 6.23: Final position of the winglet for a gust with AoA 11.5° as a function of the spring rigidity

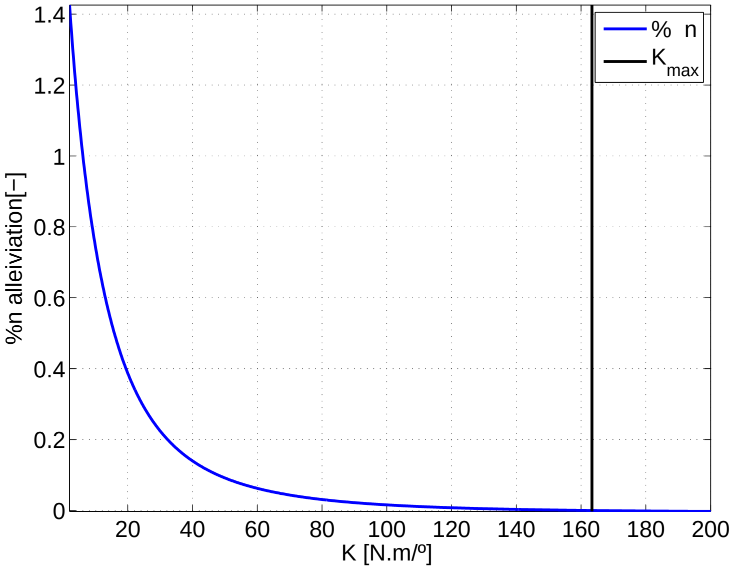

Figure 6.24: Load factor alleviation for a gust with AoA 11.5º as a function of the spring rigidity

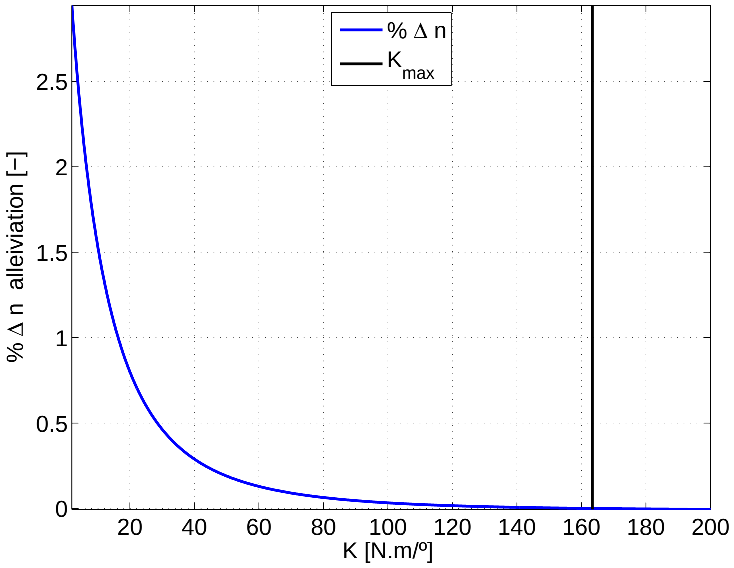

Figure 6.25: Load factor change alleviation for a gust with AoA 11.5º as a function of the spring rigidity

Figure 6.24 shows the percentage of load factor alleviation as a function of K. In this picture it can also be seen the range of values that K can adopt. For the highest calculated value of K, the percentage of assuagement is exactly 0, since there are no benefits in having a load factor higher than the one of a rigid winglet. Figure 6.25 shows the percentage of mitigation of the change in load factor between cruise and gust. It follows a similar pattern as the previous Figure, but the alleviation of the change is higher in percentage.

By looking together at Figures 6.22, 6.24 and 6.25, it can be concluded that **the more flexible the winglet is, the highest is the load alleviation of the aircraft**. With the allocation of a spring between the wing and winglet, the assuagement of total load factor can be of the order of a 1%, and the mitigation of the increase in load from cruise is of the order of a 2%. This could benefit the aircraft since it may reduce the weight of the structure by a similar percentage, fact that should be studied in further developments.

Now, the evolution of load factor with time is presented. Also, the change of Lift and Drag coefficient as well as load factor with Angle of Attack are showed. The intermediate Angles of Attack selected between 4.5 and 11.5 are 6, 6.7, 7.4, 8.1, 8.8 and 9.5 °. All the results for these Angles of Attack can be seen in Appendix A.

Figure 6.26 shows the load factor as a function of time. In it, there are two lines, one for a winglet in which the Cant Angle is fixed in 8.6 and other in which the winglet is flexible with a stiffness of 2 N.m/° (These two conditions are maintained in the following three figures). It can be seen how its shape resembles a $(1-\cos)$ function as expected from the proposed shape of a gust by regulations. It is appreciated how the evolution for load factor is almost equal for rigid and passive winglet for the majority of the gust, being a bit lower for the flexible case. However, at the end of the gust, in which the load is higher, the passive design results to be alleviating loads in a higher percentage.

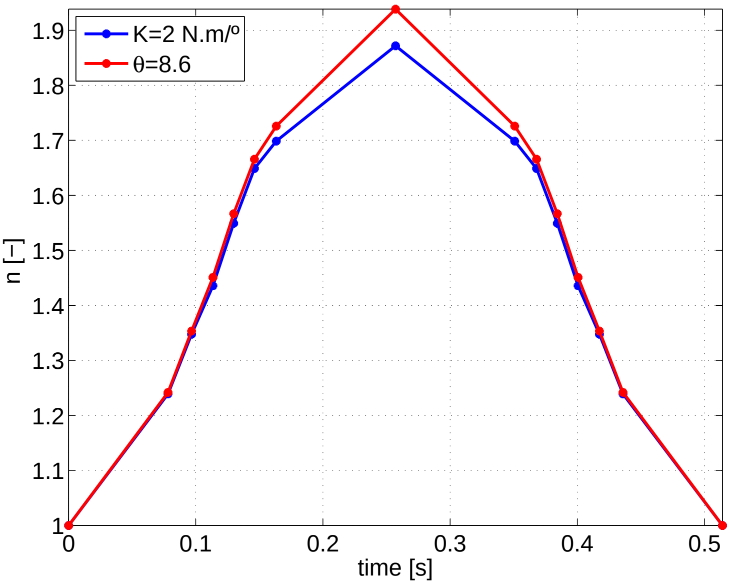

Figure 6.26: Load factor factor evolution with time for a gust of 11.5 °

Figure 6.27 shows the evolution with Angle of Attack of Lift coefficient for the case of a rigid and a flexible winglet. Figure 6.26 shows the same plot but for the load factor. The progression of both graphs is the same for the complete gust, being the load always lower for the flexible winglet and finding the higher difference at the gust Angle of Attack.

This effect can be beneficial, since the aircraft only looses a considerable quantity of Lift when it tunes the Angle of Attack to very high values. Then, if, for instance, the airplane wants to increase the Angle of Attack to relatively low values so as to change the flight level to higher altitudes, it could do it without loosing big amounts of Lift.

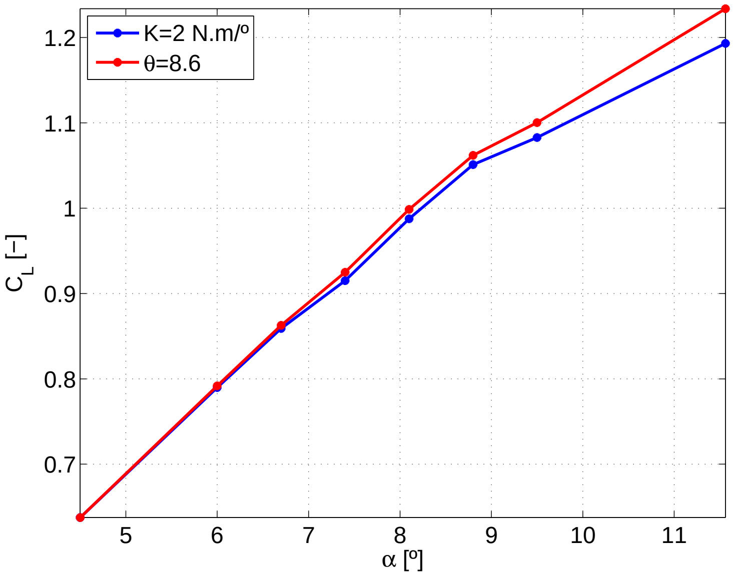

Figure 6.27: Lift coefficient as a function of AoA for rigid and flexible winglet

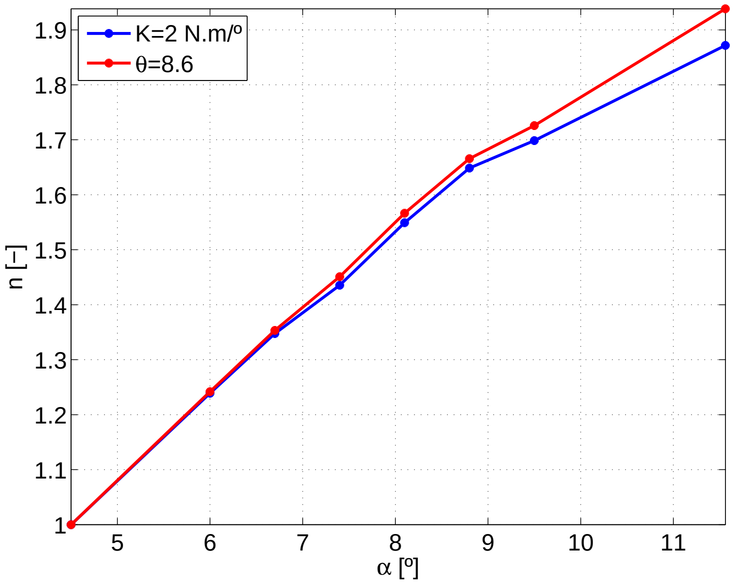

Figure 6.28: Load Factor as a function of AoA for rigid and flexible winglet

Finally, Figure 6.29 shows the Drag coefficient as function of the Angle of Attack. It can be seen how for the majority of the gust the Drag coefficient is lower for the flexible case, but it is higher at the top peak of the gust. Then, in terms of Drag the proposed design is penalized for the gust maneuver. However, this is not a major drawback since this increase on Drag is instantaneous and then the fuel consumption would not be affected.

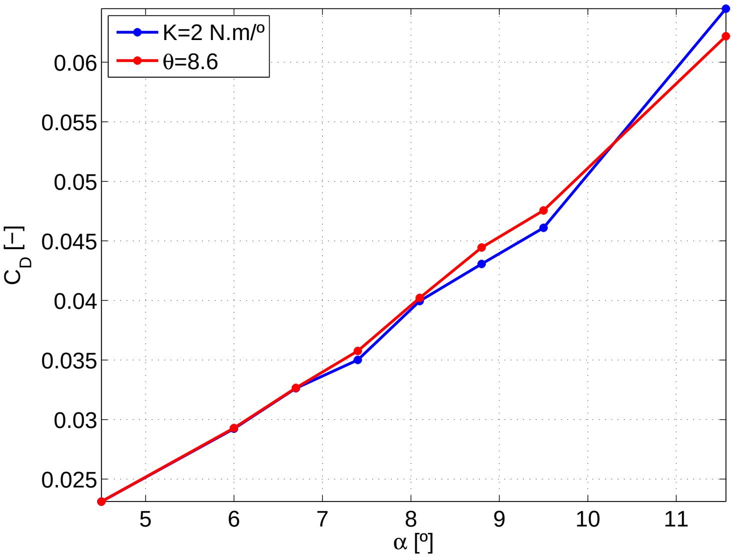

Figure 6.29: Drag coefficient as a function of AoA for rigid and flexible winglet

6.4.1 Possible drawbacks

Once that it has been seen that the more flexible the winglet is, the lower loads are found for the case of gust, some aspects have to be remarked:

- **Natural position of the spring.** The feasible values of K have to be studied in terms of the natural position of the spring that is found for each one. Natural positions lower than -90º or even higher could be problematic since the action of air could not move the winglet in the desired direction[2] under some circumstances. If low rigidities are feasible in structural terms, kind of a new design device that maintains the position at another Cant Angle different than the natural position when the airplane is not flying (forcing in this way the natural position to be a different one) could be implemented so as to have the higher possible load alleviation factors.
- **Structural integrity.** It has been seen that the lower is the rigidity of the spring, the best it is in terms of loads. Nevertheless, this could be not feasible in terms of the structural integrity of the wing, since a very flexible winglet could transform into instability of the whole airplane.
- **Aeroelasticity.** The effect that the presented winglet would have on phenomena like flutter has to be assessed. This is because it may suppose a change in the normal modes of the wing, which could affect this phenomenon.

6.5 Active design analysis

In this case, as explained before, the final position of the winglet is selected to be at 80 degrees, producing the lowest load factor for the gust condition. This final load factor is $n_{gust,\theta=80^{o}} = 1.8716$, while the final load factor for the rigid case was $n_{\theta_w=8.6} = 1.9384$. By looking at both, it can be seen how the active case produces a lower load factor than the passive case. Then, in a first approach, the active case provides higher alleviation than the passive case. The mitigation of the total load factor is a **3.4433%** of the final load, which is of the order of three times the assuagement achieved with the passive case. The abatement of the change in load factor with the cruise as reference is **7.1126%**. The computed load reduction could be so beneficial for the aircraft structure due to the high reductions in weight that it could produce. However, in this case the alleviation of the total load is not so clear, due to the fact that the weight of the needed system to actuate the winglet should be balanced with the decrease in weight that it produces.

---

[2] The desired direction, looking straight at the airplane nose would be clockwise in the wing in our left and counter-clockwise in the wing in our right.

In order to compute the variation of moment with Cant Angle it is necessary to follow equation 5.14 proposed in the mathematical procedure. The constants are: $c_1 = -7.0645$ and $c_2 = 590.9815$. After computing these constants, the equilibrium point for a set of Angles of Attack is computed following a similar procedure as for the passive case in the state of gust. The intersection between the line of equation 5.14 and the curve of moment vs Cant Angle for each Angle of Attack is the equilibrium. With this, the evolution of all the forces can be computed as a function of time and Angle of Attack.

Figure 6.30 shows the evolution of the load factor with time for the rigid and active case. It can be seen how it adopts a (1-cos) shape as expected from equation 1.1.

It is appreciated how the load factor is lower at each point when the winglet is active. The highest difference is found at the peak of this graph at which it is found the mentioned 3.4433 %.

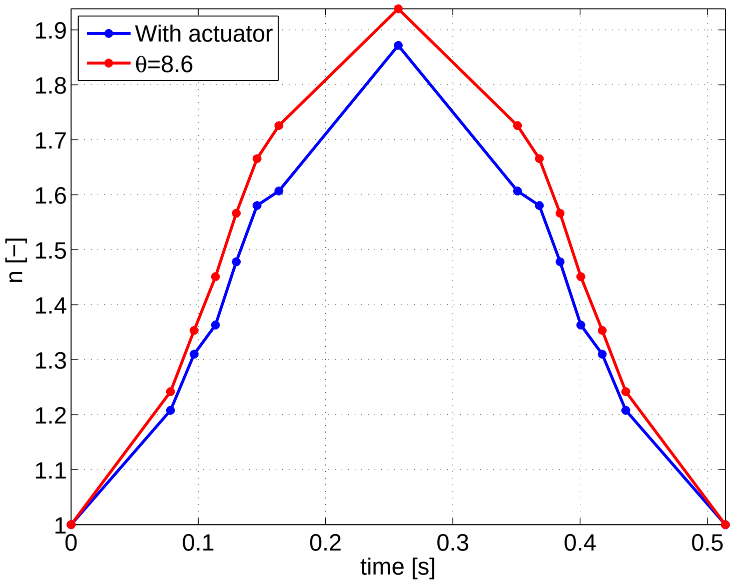

Figure 6.30: Load factor factor evolution with time for a gust of 11.5 ^{o}

Figure 6.31 shows the evolution of the Lift coefficient with the Angle of Attack. It is seen that the produced Lift is lower at every point of the graph, so it is lower for each Angle of Attack. Figure 6.32 shows the same evolution but for the load factor instead of the Lift coefficient. Both graphs follow the same evolution. On Figures 6.30, 6.31 and 6.32 it is seen how the loads at each point are lower for the active case than for the passive case.

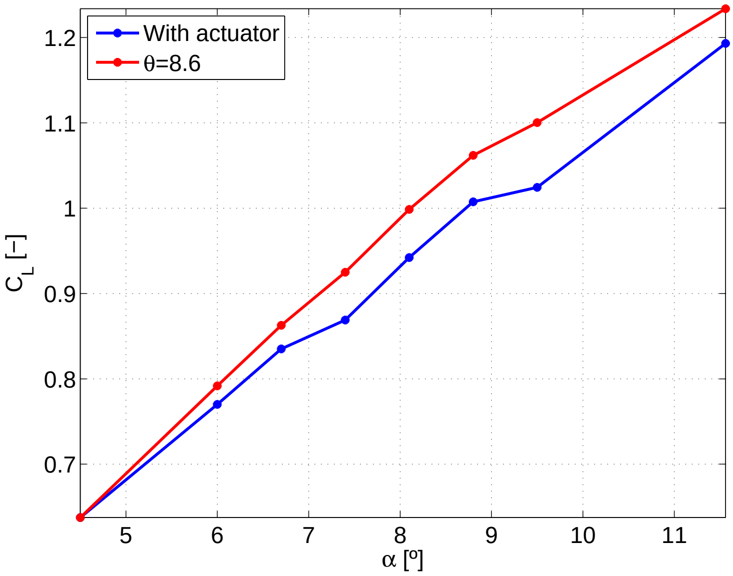

Figure 6.31: Lift coefficient as a function of AoA for rigid and actuated winglet

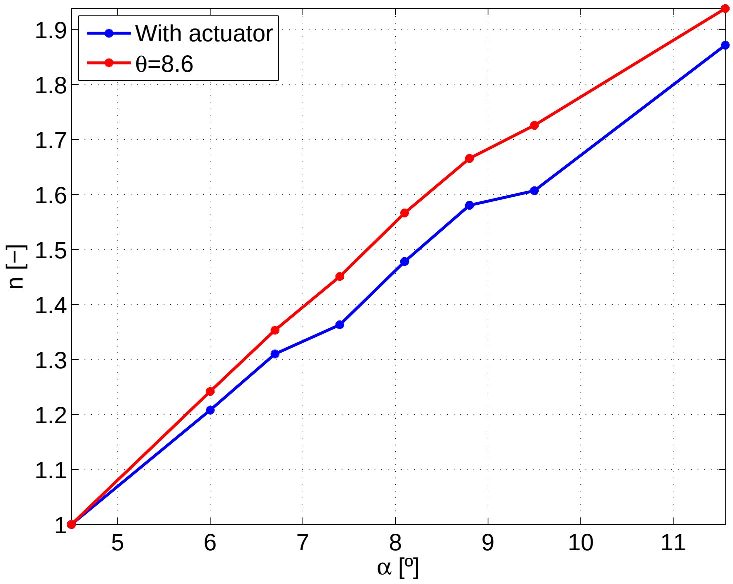

Figure 6.32: Load Factor as a function of AoA for rigid and actuated winglet

It is also of interest to look at Figure 6.33, which presents the evolution of the Drag coefficient with the Angle of Attack. It is seen that in terms of Drag, the active design penalizes the aircraft performance since it provides a higher Drag for the gust condition. This is due to the peak that was seen in the plots of the Drag as a function of the winglet angle. When the selected angle for gust is the highest one, it produces the lowest load factor, but also the Drag goes to its highest peak.

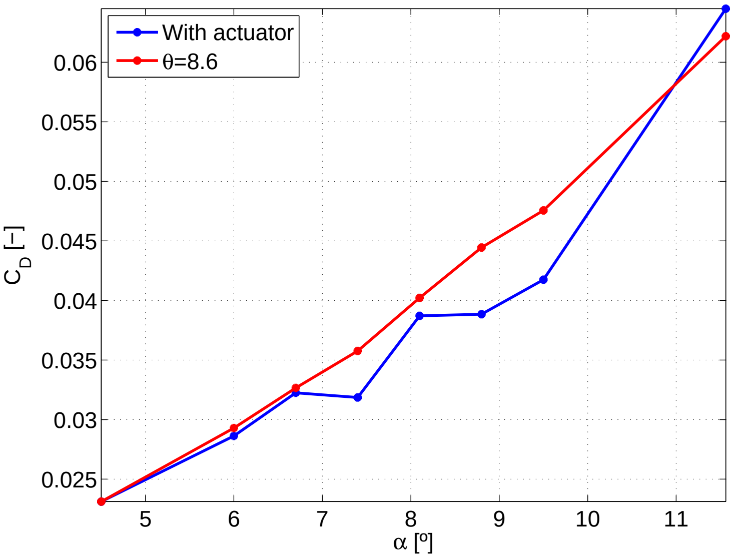

Figure 6.33: Drag coefficient as a function of AoA for rigid and actuated winglet

Chapter 7

Project Budget and Planning

7.1 Budget

The budget is a summary of all the costs associated with the current project. Its main goal is the possible future reduction of the total money wasted in order to optimize even more the economic perspective. They were needed in order to implement the project a Personal Computer for running the simulations, a Laptop for the data processing and an ANSYS license. The hours needed for all the simulations include all the hours dedicated to non-productive simulations. These are the non-valid simulations due to some errors in the set-up or in the computer. It is also considered that the computer running at its maximum performance wastes 200 W per hour.

Principal costs	
ANSYS Research license	2500 €
Matlab Academic License	500 €
Personal Computer	800 €
Laptop	600 €
Total	**4400 €**

Table 7.1: Principal costs

Working Hours	
Research time	15 h
ANSYS learning hours	30 h
Grid Independence Study	50 h
Set up time	100 h
Data processing	60 h
Thesis writing	100 h
Total working hours	**355 h**
Simulations running time	700 h

Table 7.2: Working Hours

Working prices	
Labour cost (€/h)	25
Electricity cost (€/kWh)	0.13

Table 7.3: Working prices

Total costs	
Electricity costs	18.2 €
Principal costs	4400 €
Labour costs	8875 €
TOTAL	**13293.2 €**

Table 7.4: Final Budget

7.2 Planning

The planning of the project can be seen in Figure 7.1. It is stated by means of a Gantt diagram. On it, the expected start weeks and duration for each task are written. Also, the actual start week and real period are summarized.

It is possible to see how the major problem with the current project was the running of the simulations. This is due to the fact that in many occasions, when running the simulation, the Set-up of each case was wrong. this was realized after running the calculation, and then there was a lot of time wasted in this way. Due to this delay, the thesis writing and the data analysis had to be also postponed until the real end of the simulations, as it was planified.

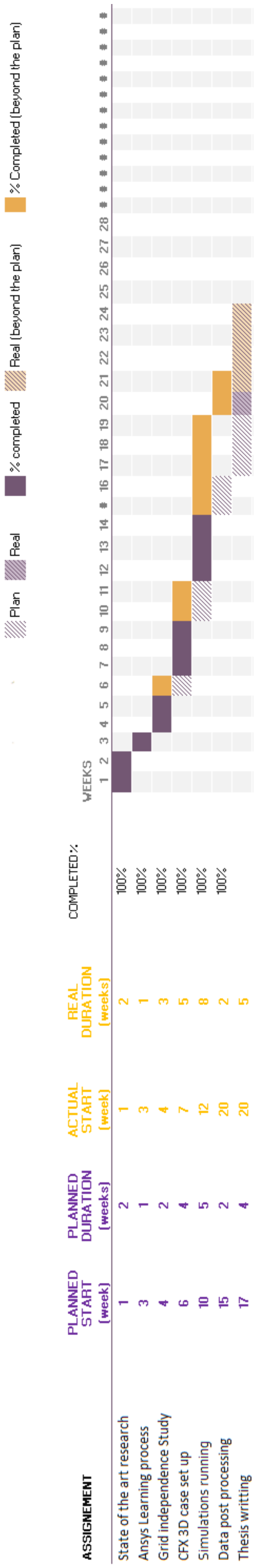

ASSIGNEMENT	PLANNED START (week)	PLANNED DURATION (weeks)	ACTUAL START (week)	REAL DURATION (weeks)	COMPLETED %
State of the art research	1	2	1	2	100%
Ansys Learning process	3	1	3	1	100%
Grid independence Study	4	2	4	3	100%
CFX 3D case set up	6	4	7	5	100%
Simulations running	10	5	12	8	100%
Data post processing	15	2	20	2	100%
Thesis writting	17	4	20	5	

Figure 7.1: Gantt Diagram of the project

Chapter 8

Conclusion

To end up, several conclusions can be inferred from the project and the goals established in the introduction.

- **Main objective.** The main objective of this project was to evaluate the load alleviation produced by a flexible winglet in the presence of gusts. For doing so, a simplified structural model in which the only variable was the rigidity of a spring between the wing and the winglet was implemented. This goal was achieved through the results presented in section 6.4. Within the findings of these results, it can be seen how the final load factor can be reduced by percentages of the order of a 1% when the winglet is flexible. The principal conclusion for this is that **the more flexible the winglet is, the higher the load reduction for the case of a gust is discovered.** Besides, it has been seen in section 6.4.1 that the more flexible the winglet is, the higher number of problems can be originated in terms of structural feasibility or aeroelasticity. Then, once the solution of the more flexible winglet has shown better capabilities for the aircraft performance in gusts, its doability in reference to these circumstances has to be examined. In addition, the decrease in weight that this improvement creates has to be estimated in further advancements.

- **Secondary objectives.** There are a set of secondary objectives underlying the primary goal:
  - Prior to beginning with all the simulations in the CFX environment, a training time with this software was needed. It can be concluded that although for the purpose of the present study the achieved management of the program was good enough, for more complex studies a higher degree of understanding and dominion of CFX is essential.
  - For the post-processing of results, one main conclusion has to be made. Although the computed data with the CFD simulations was enough so as to do a complete study, it is required a higher number of simulations so as to be more precise. If more data points are computed, then the uncertainty of the performed interpolations would be lower.
  - The active system showed better performances in terms of the load reduction that it produces with respect to the passive flexible winglet. Nevertheless, the main drawback with respect to the passive case is the possible weight increase that the needed system to actuate the winglet can create. This, added to the complexity compared to the relative easy elaboration of the flexible design

makes it not to be as good as it seems at first sight. Both approaches should be analyzed in future researches.

8.1 Future work

As it has been seen, the loads can be alleviated with the inclusion of a spring between the wing and the winglet. However, more studies have to be made so as to assess the real possibility of including this type of flexible device.

First of all, the workability of this design under real flight conditions has to be evaluated. As explained in the results proposition, this design may have problems regarding the structural and aeroelastic standpoint. Then, a future development has to be made for studying the feasibility of this winglet regarding these aspects. As seen before, the more flexible the winglet is, the lower the natural Cant Angle is. Then, if the inclusion of a spring with low rigidity is proved to be feasible, it would be needed a new device which maintains the winglet under motionless conditions at a reasonable angle so that it adapts correctly to the cruise and gust conditions.

Besides, some improvements could be accomplished since the proposed geometry was not optimized. In future developments for real implementation of this design, parametric studies regarding the wing and winglet geometry have to be performed so that the system is even more optimum, and higher load alleviations are achieved.

The most important point is to relate the calculated reduction in loads with the consequent decrease in weight, and the resulting reduction in fuel consumption. This task should be performed with a more detailed study of the loads on each part of the wing structure.

Furthermore, the specifications for the actuated design should be proposed according to the needed characteristics based on this model. Moreover, the abatement in loads that this system creates, which is higher than that of the flexible case, has to be balanced with the weight addition of the needed system.

Appendices

Appendix A

Additional Figures

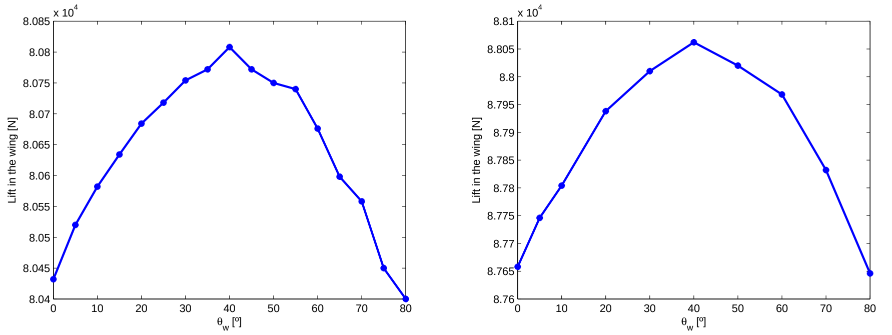

(a) Lift in the wing as a function of the Cant Angle for an Angle of Attack of 6°

(b) Lift in the wing as a function of the Cant Angle for an Angle of Attack of 6.7°

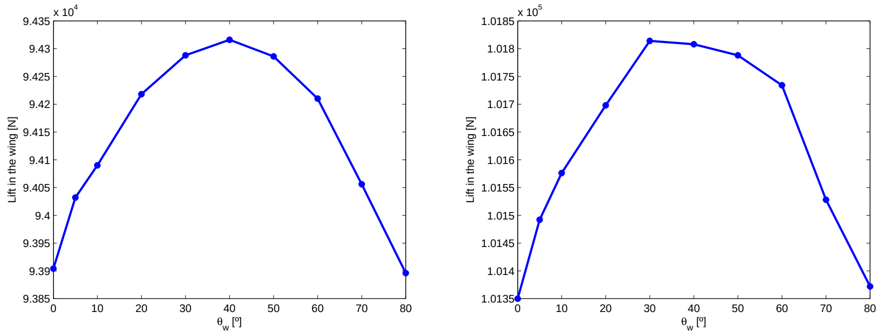

(c) Lift in the wing as a function of the Cant Angle for an Angle of Attack of 7.4°

(d) Lift in the wing as a function of the Cant Angle for an Angle of Attack of 8.1°

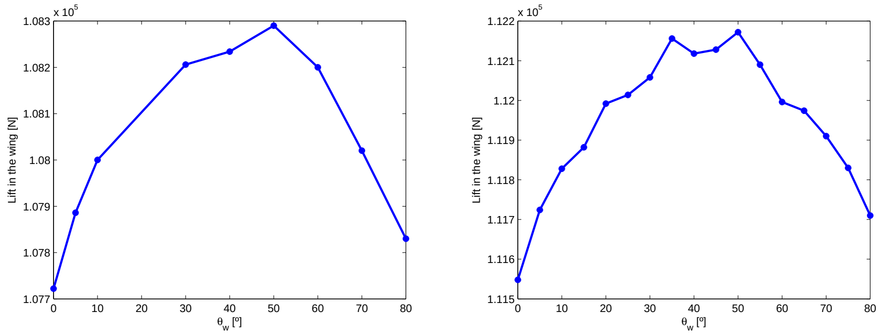

(e) Lift in the wing as a function of the Cant angle for an Angle of Attack of 8.8°

(f) Lift in the wing as a function of the Cant Angle for an Angle of Attack of 9.5°

Figure A.1: Lift in the wing as a function of the Cant Angle for a set of AoA

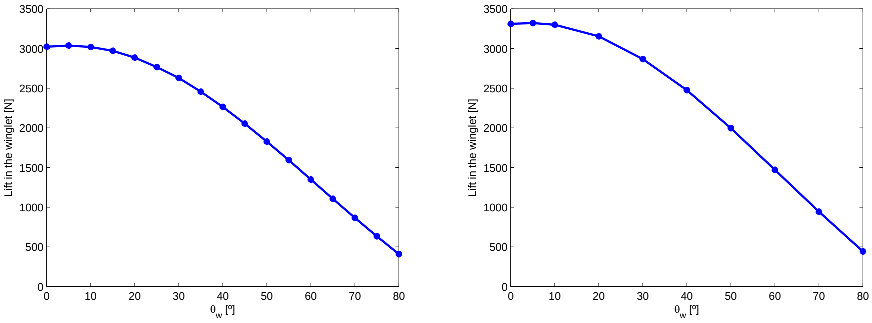

(a) Lift in the winglet as a function of the Cant Angle for an Angle of Attack of 6°

(b) Lift in the winglet as a function of the Cant Angle for an Angle of Attack of 6.7°

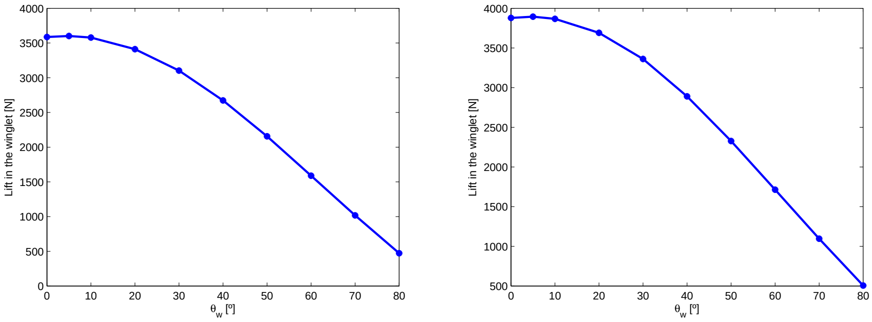

(c) Lift in the winglet as a function of the Cant Angle for an Angle of Attack of 7.4°

(d) Lift in the winglet as a function of the Cant Angle for an Angle of Attack of 8.1°

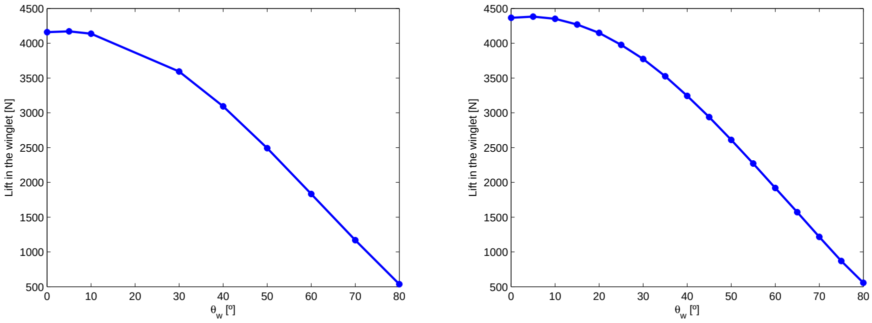

(e) Lift in the winglet as a function of the Cant Angle for an Angle of Attack of 8.8°

(f) Lift in the winglet as a function of the Cant Angle for an Angle of Attack of 9.5°

Figure A.2: Lift in the winglet as a function of the Cant Angle for a set of AoA

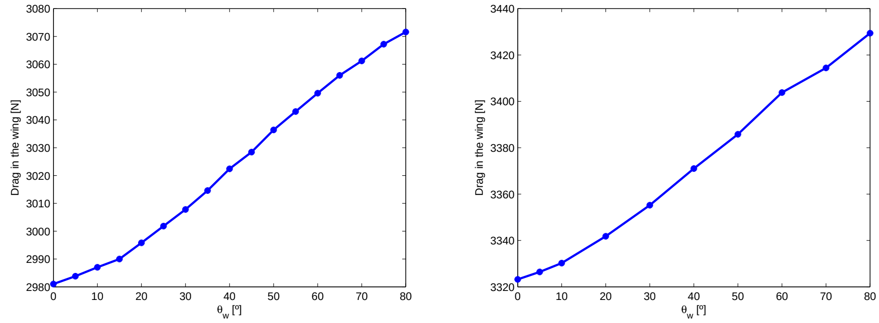

(a) Drag in the wing as a function of the Cant Angle for an Angle of Attack of 6°

(b) Drag in the wing as a function of the Cant Angle for an Angle of Attack of 6.7°

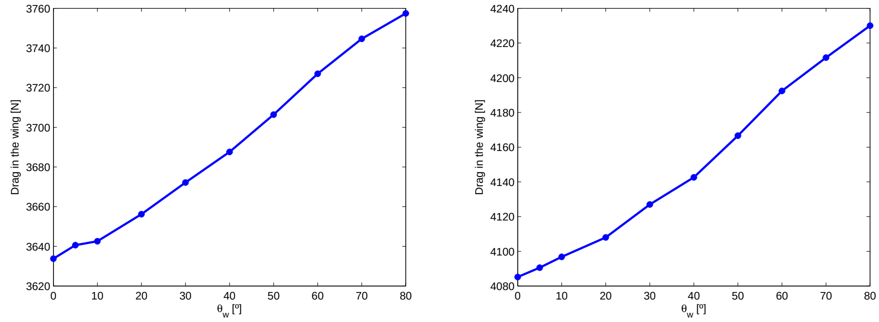

(c) Drag in the wing as a function of the Cant Angle for an Angle of Attack of 7.4°

(d) Drag in the wing as a function of the Cant Angle for an Angle of Attack of 8.1°

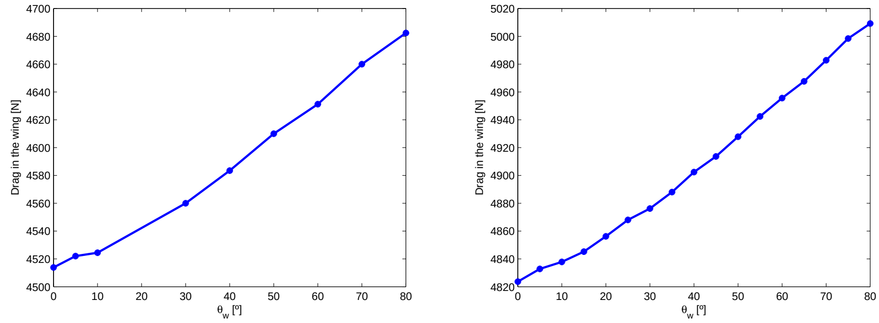

(e) Drag in the wing as a function of the Cant Angle for an Angle of Attack of 8.8°

(f) Drag in the wing as a function of the Cant Angle for an Angle of Attack of 9.5°

Figure A.3: Drag in the wing as a function of the Cant Angle for a set of AoA

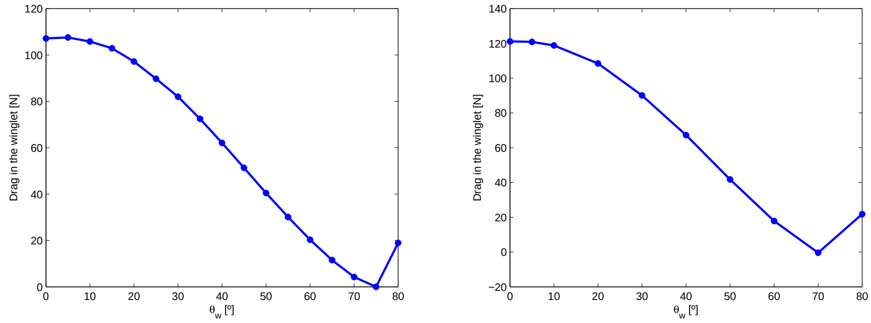

(a) Drag in the winglet as a function of the Cant Angle for an Angle of Attack of 6°

(b) Drag in the winglet as a function of the Cant Angle for an Angle of Attack of 6.7°

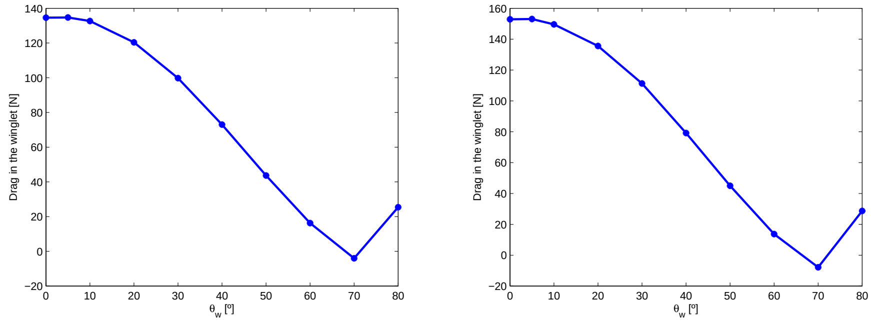

(c) Drag in the winglet as a function of the Cant Angle for an Angle of Attack of 7.4°

(d) Drag in the winglet as a function of the Cant Angle for an Angle of Attack of 8.1°

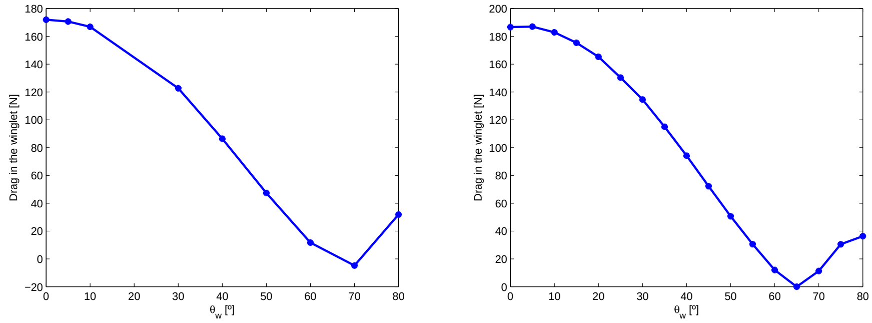

(e) Drag in the winglet as a function of the Cant Angle for an Angle of Attack of 8.8°

(f) Drag in the winglet as a function of the Cant Angle for an Angle of Attack of 9.5°

Figure A.4: Drag in the winglet as a function of the Cant Angle for a set of AoA

Bibliography

[1] Airbus, S. A. S. (2015). Global Market Forecast 2015-2034. Blagnac Cedex, France.

[2] Rajendran, S. (2012). *Design of Parametric Winglets and Wing tip devices: A Conceptual Design Approach.*

[3] Raymer, D. P. (1999). *Aircraft design: A conceptual approach*, American Institute of Aeronautics and Astronautics. Inc., Reston, VA.

[4] Myilsamy, D., Thirumalai, Y., & Premkumar, P. S. *Performance Investigation of an Aircraft Wing at Various Cant angles of Winglets using CFD Simulation.*

[5] Abdelghany, E. S., Khalil, E. E., & Abdellatif, O. E. Gamal elhariry (2016) *Aircraft Winglet Design and Performance: Cant Angle Effect.* J Robot Mech Eng Resr, 1(3), 28-34.

[6] Guo, S., Los Monteros, D., Espinosa, J., & Liu, Y. (2015). *Gust Alleviation of a Large Aircraft with a Passive Twist Wingtip.* Aerospace, 2(2), 135-154.

[7] Shijun Guo and Otto Sensburg *Passive Gust Alleviation for a Flying Wing Aircraft* Air Force Research Laboratory Air Force Office of Scientific Research European Office of Aerospace Research and Development Unit 4515 Box 14, APO AE 09421.

[8] Ursache, N. M., Melin, T., Isikveren, A. T., & Friswell, M. I. (2007, September). *Morphing winglets for aircraft multi-phase improvement.* In 7th AIAA ATIO Conf, 2nd CEIAT Int'l Conf on Innov & Integr in Aero Sciences, 17th LTA Systems Tech Conf.

[9] Bourdin, P., Gatto, A., & Friswell, M. I. (2006, June). *The application of variable cant angle winglets for morphing aircraft control.* In 24th Applied Aerodynamics Conference (pp. 5-8).

[10] Barbarino, S., Bilgen, O., Ajaj, R. M., Friswell, M. I., & Inman, D. J. (2011). *A review of morphing aircraft.* Journal of Intelligent Material Systems and Structures, 22(9), 823-877.

[11] Spalart, P. R., & Allmaras, S. R. (1992). *A one equation turbulence model for aerodinamic flows.* AIAA journal, 94.

[12] EASA, C. S. (2009). Acceptable Means of Compliance for Large Aeroplanes CS-25. Tech. Rep. Amendment 6, European Aviation Safety Agency.

[13] FAA, A. C. (2014). Airworthiness Standards: Transport Category Airplanes AC-25.341-1, Federal Aviation Administration.

[14] Rutherford, D., & Zeinali, M. (2009). *Efficiency Trends for New Commercial Jet Aircraft 1960 to 2008.*

[15] Tuncer Cebeci, *Analysis of Turbulent Flows* ISBN: 978-0-08-044350-8

[16] Dinesh, M., Kenny Mark, V., Dharni Vasudhevan Venkatesan, S. K. B., & Sree Radesh, R. (2014). *Diagnostic investigation of aircraft performance at different winglet cant angles.* World Acad. Sci. Eng. Technol., 8.

[17] Leishman, J. G. (2002, January). *Challenges in modeling the unsteady aerodynamics of wind turbines.* In ASME 2002 Wind Energy Symposium (pp. 141-167). American Society of Mechanical Engineers.

[18] ANSYS, I. (2009). ANSYS CFX Introduction. Canonsburg, PA.

[19] ANSYS, I. (2009). ANSYS CFX-Solver theory guide. Canonsburg, PA.

[20] ANSYS, I. (2009). ANSYS CFX-Solver modeling Guide. Canonsburg, PA.

[21] ANSYS, I. (2013). ANSYS Meshing User's guide. Canonsburg, PA.

[22] ANSYS, I. (2009). CFX-Mesh. Canonsburg, PA.

[23] ANSYS, I. (2009). ANSYS CFX Reference Guide. Canonsburg, PA.